NASA Contractor Report 2993

High Angle Canard Missile Test in the Ames 11-Foot Transonic Wind Tunnel

Richard G. Schwind

CONTRACT NAS2-9211
JUNE 1978

NASA

NASA Contractor Report 2993

High Angle Canard Missile Test in the Ames 11-Foot Transonic Wind Tunnel

Richard G. Schwind
Nielsen Engineering & Research, Inc.
Mountain View, California

Prepared for
Ames Research Center
under Contract NAS2-9211

National Aeronautics
and Space Administration

Scientific and Technical Information Office

1978

TABLE OF CONTENTS

LIST OF TABLES

LIST OF FIGURES

LIST OF FIGURES (CONTINUED)

LIST OF FIGURES (CONCLUDED)

HIGH ANGLE CANARD MISSILE TEST IN THE AMES 11-FOOT TRANSONIC WIND TUNNEL

by Richard G. Schwind
Nielsen Engineering & Research, Inc.

SUMMARY

Four blunted ogive-cylinder missile models with a length-to-diameter ratio of 10.4 have been tested at transonic speeds and large angles of attack in the NASA/Ames Research Center Unitary Plan 11-Foot Transonic Wind Tunnel. The configurations are: body, body with tail panels, body with canards, and body with canards and tails. Forces and moments from the entire model and each of the eight fins were measured over the pitch range of 20° to 50° and 0° to 45° roll. Canard deflection angles between 0° and 15° were tested. Exploratory vapor screen flow visualization testing was also performed. Sample force and moment data are reported along with observations from the vapor screen tests. Comparisons made of body and panel loads for the same models tested previously in the Ames 6- by 6-Foot Wind Tunnel showed good agreement in a small overlapping range of pitch angles.

INTRODUCTION

Tests of a canard-cruciform missile model were conducted in the NASA/Ames Research Center Unitary Plan 11-Foot Transonic Wind Tunnel during October and November 1976. Force and moment data were obtained along with some experimental vapor screen motion pictures. Tests were performed at unit Reynolds numbers between 3.9 and 13.5 million per meter (1.2 and 4.1 million per foot) at Mach numbers of 0.8, 1.22, and 1.3. Four model configurations were tested at pitch angles between 20° and 50° using four combinations of canard pitch angles and five roll angles. The model was a blunted ogive-cylinder body of 0.127-meter (5-inch) diameter by 1.32 meters (52 inches) long. It was loaned to NASA for these tests by Mr. Ray Deep of the U. S. Army Missile Command (MICOM). The same model configurations were tested in June 1974 in the Ames 6- by 6-Foot Supersonic Wind Tunnel at pitch angles of 0° to 24°.

The purpose of the test was to obtain a data base for comparison of theory to experiment at the extended pitch range of 20° to 50°. The theoretical techniques will, in turn, be available for future missile

design. An unusual set of scheduling circumstances in this very busy wind tunnel made it possible to experiment with the vapor screen flow visualization technigue. For the first time vapor screen pictures were obtained in this wind tunnel. These results are expected to add to the understanding of the flow field and thereby to aid in a concurrent analytical investigation at Nielsen Engineering & Research, Inc. (NEAR).

This test report documents the data taken during the tests in sufficient detail to permit their use by others. A comprehensive set of DATAMAN plots that resulted from this test are reported in a separated document (ref. 3). The list of symbols of this report includes the notations used for both the computer data listing and the plots. The test apparatus and procedures are detailed in section 3. The aerodynamic coefficients are defined in chapter 4, sample results are presented in chapter 5, and conclusions noted in chapter 6.

The excellent services of the test engineer, Mr. Clyde Allen, NASA/Ames Experimental Investigations Branch, are acknowledged.

LIST OF SYMBOLS

SYMBOL	COMPUTER LISTING SYMBOL	COMPUTER PLOT SYMBOL	DEFINITION
a	---	---	Body radius at panel attachment point 0.06350 meter (0.20833 ft.).
A	---	---	Missile axial force measured along body centerline by main balance. See figure 8 for sign convention.
$b_{C,T}$	---	---	Distance from panel hinge line to body moment center (station 26), (see fig. 8). For the canard panel attachment points, b_C = 0.2794 meters (0.916667 ft.); for the tail panel attachment points, b_T = 0.508 meters (1.66667 ft.).
BM_{C_j,T_j}	---	---	Root chord bending moment for canard or tail panel number j measured about an axis through the panel attachment point (at the body), perpendicular to the panel hinge line, and in the plane of the panel planform, (see fig. 9); j = 1,2,3,4.
C_A	CA	C_A	Missile axial-force coefficient in unrolled body axis system. See figure 8 for sign convention. $C_A = A/S_{ref}q$
$C_{BM_{C_j,T_j}}$	CBMCj CBMTj	CBMCj CBMTj	Root chord bending-moment coefficient for panel j measured about an axis through the panel attachment point (at the body), perpendicular to the panel hinge line, and in the plane of the panel planform (see fig. 9); j = 1,2,3,4. $C_{BM_{C_j,T_j}} = BM_{C_j,T_j}/S_{ref}q\ell_{ref}$
$C_{HM_{C_j,T_j}}$	CHMCj CHMTj	CHMCj CHMTj	Hinge-moment coefficient for canard or tail fin number j measured about the panel hinge line which is perpendicular to the body axis (see fig. 9). $C_{HM_{C_j,T_j}} = HM_{C_j,T_j}/S_{ref}q\ell_{ref}$

LIST OF SYMBOLS (Continued)

SYMBOL	COMPUTER LISTING SYMBOL	COMPUTER PLOT SYMBOL	DEFINITION
C_{ℓ}	CRM	C_{ℓ}(BODY)	Missile rolling-moment coefficient obtained from main balance. Measured about body longitudinal axis. See figure 8. $C_{\ell} = M_{\ell}/S_{ref}q\ell_{ref}$
$C_{\ell_{C(B)}}$	CRMC	CRMC	Rolling-moment coefficient in body axis system for canard panels taken together. Defined by equation (6).
$C_{\ell_{C(B)+T(B)}}$	CRMB	CRMB	Rolling-moment coefficient in body axis system for all canard and tail panels taken together. Defined by equation (16).
$C_{\ell_{T(B)}}$	CRMT	CRMT	Rolling-moment coefficient in body axis system for tail panels taken together. Defined by equation (11).
C_m	C_M	C_m	Missile pitching-moment coefficient measured in unrolled body axis system, $C_m = M_m/S_{ref}q\ell_{ref}$ (see fig. 8).
$C_{m_{C(B)}}$	CMC	CMC	Pitching-moment coefficient in unrolled body axis system for canard panels taken together. Defined by equation (4).
$C_{m_{C(B)+T(B)}}$	CMB	CMB	Pitching-moment coefficient in unrolled body axis system for all canard and tail panels taken together. Defined by equation (14).
$C_{m_{T(B)}}$	CMT	CMT	Pitching-moment coefficient in unrolled body axis system for tail panels taken together. Defined by equation (9).
C_N	CN	C_N	Missile normal-force coefficient in unrolled body axis system. See figure 8 for sign convention. $C_N = N/S_{ref}q$

LIST OF SYMBOLS (Continued)

SYMBOL	COMPUTER LISTING SYMBOL	COMPUTER PLOT SYMBOL	DEFINITION
$C_{N_{C_j,T_j}}$	CNCj CNTj	CNCj CNTj	Normal-force coefficient for canard or tail fin number j. Force measured normal to panel planform. See figure 9. $C_{N_{C_j,T_j}} = N_{C_j,T_j}/S_{ref}q$
$C_{N_{C(B)}}$	CNC	CNC	Normal-force coefficient in unrolled body axis system for canard panels taken together. Defined by equation (2).
$C_{N_{C(B)+T(B)}}$	CNB	CNB	Normal-force coefficient in unrolled body axis system for all canard and tail panels taken together. Defined by equation (12).
$C_{N_{T(B)}}$	CNT	CNT	Normal-force coefficient in unrolled body axis system for tail panels taken together. Defined by equation (7).
C_n	CYM	C_n(BODY)	Missile yawing-moment coefficient in unrolled body axis system. See figure 8 for sign convention. $C_n = M_n/S_{ref}q\ell_{ref}$
$C_{n_{C(B)}}$	CYMC	CYMC	Yawing-moment coefficient in unrolled body axis system for canard panels taken together. Defined by equation (5).
$C_{n_{C(B)+T(B)}}$	CYMB	CYMB	Yawing-moment coefficient in unrolled body axis system for all canard and tail panels taken together. Defined by equation (15).
$C_{n_{T(B)}}$	CYMT	CYMT	Yawing-moment coefficient in unrolled body axis system for tail panels taken together. Defined by equation (10).
CPX_{C_j,T_j}	CPXCj CPXTj	CPXCj CPXTj	Ratio of chordwise distance to panel center of pressure to reference length for canard or tail fin number j, measured from hinge line positive aftward (see fig. 9). $CPX_{C_j,T_j} = -HM_{C_j,T_j}/N_{C_j,T_j}\ell_{ref}$

LIST OF SYMBOLS (Continued)

SYMBOL	COMPUTER LISTING SYMBOL	COMPUTER PLOT SYMBOL	DEFINITION
CPXN	CPXN	CPXN	Axial center of pressure for normal force, unrolled body coordinates, from MS=0, non-dimensionalized by reference length, ℓ_{ref}. $CPXN = 5.2 - C_m/C_N$
CPXY	CPXY	CPXY	Same as above but for side force. $CPXY = 5.2 - C_n/C_Y$
CPY_{C_j,T_j}	CPYCj CPYTj	CPYCj CPYTj	Ratio of spanwise distance to panel center of pressure to reference length for canard or tail fin number j, measured from body surface at attachment point (see fig. 9). $CPY_{C_j,T_j} = BM_{C_j,T_j}/N_{C_j,T_j}\ell_{ref}$
CRM_{C_j,T_j}	CRMCj CRMTj	CRMCj CRMTj	Rolling-moment coefficient for canard or tail fin number j. Defined by equation (1). (For is taken in the same sense as positive bending moment).
C_Y	CY	C_Y	Missile side-force coefficient in unrolled body axis system (see fig. 8). $C_Y = Y/S_{ref}q$
$C_{Y_{C(B)}}$	CYC	CYC	Side-force coefficient in unrolled body axis system for canard panels taken together. Defined by equation (3).
$C_{Y_{C(B)+T(B)}}$	CYB	CYB	Side-force coefficient in unrolled body axis system for canard and tail panels taken together. Defined by equation (13).
$C_{Y_{T(B)}}$	CYT	CYT	Side-force coefficient in unrolled body axis system for tail panels taken together. Defined by equation (8).

LIST OF SYMBOLS (Continued)

SYMBOL	COMPUTER LISTING SYMBOL	COMPUTER PLOT SYMBOL	DEFINITION
HM_{C_j,T_j}	---	---	Hinge moment for canard or tail fin number j measured about the panel hinge line which is perpendicular to the body axis, (see fig. 9 for sign convention).
ℓ_{ref}	---	---	Reference length for all coefficients, 0.1270 meters (0.416667 ft.) (missile body diameter for cylindrical portion).
M	MACH	MACH	Mach number.
M_ℓ	---	---	Missile rolling moment in unrolled body axis system. See figure 8 for sign convention.
M_m	---	---	Missile pitching moment in unrolled body axis system. See figure 8 for sign convention.
M_n	---	---	Missile yawing moment in unrolled body axis system. See figure 8 for sign convention.
N	---	---	Missile normal force in unrolled body axis system. See figure 8 for sign convention.
N_{C_j,T_j}	---	---	Normal force for canard or tail fin number j. Force measured normal to panel planform (see fig. 9).
p	p	---	Free-stream static pressure, psf in data listing.
P_t	PT	---	Free-stream total pressure, psf in data listing.
q	Q	---	Free-stream dynamic pressure, psf in data listing.
Re_x	RN/L	---	Free-stream Reynolds number per unit length, millions per foot in data listing.
S_{ref}	---	---	Reference area for all coefficients, 0.01267 m^2 (0.136354 ft^2). (S_{ref} = cross-sectional area of cylindrical portion of model).

LIST OF SYMBOLS (Concluded)

SYMBOL	COMPUTER LISTING SYMBOL	COMPUTER PLOT SYMBOL	DEFINITION
Y	---	---	Missile side force in unrolled body axis system. See figure 8 for sign convention.
α_c	ALPHA	α	Included angle between model longitudinal axis and wind direction of free stream (see fig. 8).
δ_j	D_j	D_j	Deflection angle of canard panels. See figure 10 for sign convention.
ϕ	PHI-C PHI-M	PHI ϕ	Missile bank angle. See figure 8 for sign convention.

TEST APPARATUS AND PROCEDURES

Model, Balances, and Mounting

The model body was furnished by the U. S. Army Missile Command (MICOM). It was designed and fabricated by CALSPAN and is described in Cornell Aeronautical Laboratory Drawing W19-B01 dated January 1973. It consists of a three-caliber nose blunted by a 0.0142 meter (0.36-inch) radius. A cylindrical afterbody of 0.127 meter (5-inch) diameter completes the body. Neglecting the bluntness of the nose, the length is 1.32 meters (52 inches) and the length-to-diameter ratio is 10.4.

Four configurations were tested: body alone, body and tails, body and canards, and body with canards and tails. Canards were deflected in various combinations from 0° to 15°. In the previous 6- by 6-Foot Wind Tunnel tests at the Ames Research Laboratory with this missile test model (test number 66-036, see ref. 1) several different canard and tail shapes were tested. Two of these shapes were used for this test, the "Navy tail panels" (denoted there as T2) and the "Navy large canards" (denoted there as C6). They were mounted to the body in the same locations in both tests. The body-canard-tail configuration is shown in figure 1, and the canard and tail shapes are shown in figures 2 and 3, respectively. The same T2 tail panels were used as in the previous test. The canard panels were remachined to provide a small flaring out to a thicker section about the attachment point for reduced maximum stress. This bulge tapers from a 0.25 cm (0.100-inch) greater thickness than the surrounding canard to the original thickness in 0.51 cm (0.20-inch), see figure 2. This deviation in shape from the previous configuration is expected to have an insignificant effect upon the results.

The 6- by 6-Foot Wind Tunnel tests were performed at a total pressure of 27.6 kilonewtons per square meter (4 psia), while the pressure was as great as 103 kilonewtons per square meter (15 psia) for the 11-Foot Wind Tunnel tests. This required higher capacity balances than those used for the previous test. New MICOM three-component balances with a normal-force capacity of 667 newtons (150 lbs) were used for the tail balances, and three-component

canard balances with a normal-force capacity of 623 newtons (140 lbs) were supplied by Sandia. Also, a new model center body was fabricated to accommodate a larger main balance (no exterior dimensions were changed). The Ames 6.35-cm (2.5-inch) diameter, six-component Mark XIV Task balance was used. As in the previous test, the model could be rolled on this balance to 0°, 10°, 20°, 30°, and 45° (clockwise facing upstream).

Figure 4 shows a schematic, and figures 5 and 6 show photographs of how the missile was mounted in the 11-Foot Wind Tunnel to achieve a pitch range of 20° to 50°. Added onto the wind-tunnel body of revolution were: straight adaptor 0.76-meter (30-inch) extension, an available 45° strut with its top and bottom adaptors, and a newly fabricated tapered 10° bent sting (NEAR Drawing #337-002).

An eccentric ring of 10.2 cm (4 in.) by 3.6 cm (1.4 in.) long which contained eight identification lights (see fig. 6) for vapor screen pictures was mounted onto the sting several centimeters behind the missile base. A 16mm Milliken motion picture camera was mounted on its side inside a protecting box at the top of the strut as shown in figures 4, 5, and 6. The vapor screen apparatus is described in the next section.

Vapor Screen Apparatus

The NASA/Ames Research Center has a permanent mercury light slit arrangement for the 6- by 6-Foot Wind Tunnel for vapor screen flow visualization. This system was used for the previous tests with this missile model, and vapor screen results were reported in reference 2. These results have provided a very valuable insight into the vortical flow field on the leeward side of the body, showing the interaction of nose, canard, and afterbody vortices. No flow visualization system exists for the 11-Foot Wind Tunnel, and the 6- by 6-foot system cannot be adapted to this tunnel and provide an adequate light slit. Vapor screen photography had not been previously performed in the 11-foot facility.

It was decided to incorporate vapor screen flow visualization into this test program as a secondary objective even though makeshift arrangements would be necessary. For a light source an existing light slit was used that had been engineered and built by Nielsen Engineering & Research, Inc. (NEAR) and the Ames Research Center for smoke flow visualization in the 40- by 80-Foot Wind Tunnel. This light source consists of an 800-watt Xenon lamp and power supply manufactured by the Eimac Division of Varian, a light slit iris, front surface mirror, and a 0.305-meter (1-foot) square Plexiglass cylindrical lens. These elements, other than the lamp power supply, are mounted inside a 0.305-by 0.61-by 1.22-meter (1-by 2-by 4-foot) enclosure with the mirror simply folding the light path between the lamp and the lens. The lens is mounted on a track for adjusting the focus point of the light slit. This light slit box was set on an auto jack on a cart. It could be moved up and down and rolled along in tracks parallel to and 5.5 meters (18 feet) from the tunnel centerline (the minimum focus distance for the light slit), see figure 7.

Normally a light slit is oriented perpendicularly to a missile body centerline to visualize cross sections of the flow. Because of the large pitch angles of this test and a lack of appropriate equipment, the light slit orientation was kept vertical. Several other factors complicated or degraded the vapor screen flow visualization photography. They are noted here as items to be considered in any future such experiments. The 11-Foot Wind Tunnel has a large window area in the test section but it is divided into small sections of thick window panes separated by wide dividers containing the ducts for the porous wall. The test section is surrounded by a plenum with similar glass panes and dividers. These two sets of horizontal dividers create wide shadows when attempting to illuminate a cross section of the test area from outside the tunnel (see fig. 7). The vertical dividers make it impossible to illuminate certain cross sections. During the test either the light source or the model was translated vertically to move the positions of the shadow with respect to the model, then the photography was repeated. Light reflections from the four sets of windows and the light tunnel interior paint added to the

light scattering and loss of contrast. For future vapor screen experiments in this tunnel a darkened tunnel interior and a remotely controlled light source mounted in the tunnel plenum area should be considered. Camera placement was also a problem for this test. Normally the camera is mounted to the sting in such a manner as to look directly up along the leeward side of the body. The sting for this test had a 10° bend that pushed the forebody down, away from the view of the usual camera location. The camera had to be mounted to the top adapter of the strut, and so it had a downward view of the model. This caused a considerable loss of contrast, even though the model was painted flat black, and it also makes the pictures difficult to interpret.

The motion picture camera mounted to the top adapter within the protective enclosure that is seen in figures 5 and 6 was a variable speed 16mm Milliken with a 10mm f/1.8 lens and 160° shutter.

Balance Calibrations, Check Loads, and Deflections

The main balance, four tail balances, and four canard balances were calibrated at the ARC Balance Room. The appropriate coefficients for each balance were calculated by ARO, Inc. at Ames using standard procedures. The deflections of the canard balances were found to be appreciable at the maximum loads expected, so deflections were also noted. All balances were check loaded in the wind tunnel before the testing commenced. These items are described below.

The main balance was the 6.35 cm (2.5-inch) diameter, six-component Mark XIV Task balance. This balance has an exceptionally large capacity for its size: 17,800, 8,900, 17,800 newtons, and 226 newton meters (4000, 2000, 4000 lbs, and 2000 inch-pounds) for front and aft normal force, front and aft side force, axial force, and rolling moment, respectively. This large capacity balance was necessary since the balance was located quite far behind the center of pressure, resulting in large pitching moments, particularly for the canard-body configuration. This relatively rearward balance position was due to the internal space required for the canard actuation package. The balance was calibrated by standard procedures.

Check loading of the normal-force and side-force gages during the tunnel installation process showed indicated values to be within 0.2 percent of full scale of applied loads. Checking the roll gage required extra care since all four of the forward pin holes were used at one time or another as the model was rolled to its five different roll angles. Therefore, after calibrating the balance using one pin location, check loading was performed for each of the other pin locations. This showed the largest percentage variation of indicated roll to be 0.7 percent of full scale, caused by loading the forward normal-force gage to capacity. All other possible full-scale loadings created less than a 0.3 percent change in the indicated roll due to pin location.

Both the tail and canard balances were mounted in place in the test missile body for calibration. For the tail balances a standard calibration fin was attached to each balance in turn and calibration loads to 445 or 623 newtons (100 to 140 lbs) were applied at three successive locations, denoted N1, N2, and N3, and then check loads were applied at four other locations on each side. Using the model radius and the fin hinge line for a local x_f, y_f coordinate system (see figs. 2 and 3, the gap between each fin and the body is included in y_f), the N1, N2, and N3 loading positions were located as follows.

	TAILS		CANARDS	
	x_f	y_f	x_f	y_f
N1	2.54	4.059	-2.286	1.778
N2	-2.54	4.059	0.000	1.778
N3	0.00	6.162	0.00	4.572

Location of calibration and check load points, cm.

After applying each load, the fin surface was leveled before recording the measurements. The canard balances were calibrated in essentially the same manner, except each canard was centerdrilled to produce a 0.025 cm (0.010-inch)deep conical depression for locating the weight pan at each calibration point.

All canards and tails were check-loaded during the tunnel installation procedure. Example comparisons of applied and measured loads are presented in Table I. The differences are typical for these types of balances. Presumably, much of the deviation is due to the difficulty in accounting for the strong interaction between the three measured balance components. Also, the fins were not leveled after applying the load during this tunnel check-loading procedure.

The deflections of the mounting system and main balance were measured during the installation check loading of the Task balance. This information was used to correct the indicated pitch angles during testing, a correction of less than one degree.

The deflections of the canards appeared to be large at the full capacity load of 489 newtons (110 lbs) so a comprehensive set of deflection measurements were made before the tunnel entry. This consisted of measuring the displacements at three locations on each canard while loads were successively applied at N1, N2, and N3. Using a nominal center of pressure of the hinge line at 40 percent of the span, the negative loading direction for canard 1 produced a deflection there of 0.78×10^{-3} cm/newton (0.0014 in/lb), while the remaining five combinations of canards and loading directions presented a less stiff mounting of 1.14×10^{-3} cm/newton (0.002 in/lb) deflection.

The increase in the canard deflection angle $\Delta\delta$ due to the canard normal force, hinge and bending moments can be expressed as

$$\Delta\delta = \frac{\partial\delta}{\partial N}\Delta N + \frac{\partial\delta}{\partial HM}\Delta HM + \frac{\partial\delta}{\partial BM}\Delta BM$$

These coefficients were found to be (near the base of the canard):

normal force	0.9×10^{-3}	deg/newton	(0.004 deg/lb)
hinge moment	0.15	deg/newton-meter	(0.017 deg/in-lb)
bending moment	0.01	deg/newton-meter	(0.001 deg/in-lb)

for all loadings of the canards, except the negative loading of canard one, which was stiff enough so that these angular deflections were negligible.

As an example of the impact of these flexibilities, we will use data from a run at the greatest test Reynolds number, Re = 1.25×10^6 per meter (4.1×10^6 per foot, the pressure is 2.5 times the usual value for the test), at the maximum pitch angle of 50.0° for 20° roll with all canards at a nominal value of no deflection (δ's = 0). This produces large forces on canard 4 resulting in a normal-force coefficient, CNC4 = 0.635, hinge-moment coefficient, CHMC4 = 0.0297, and bending-moment coefficient, CBMC4 = 0.159. The resulting increase in canard angle from these aerodynamic loads, as calculated using the above coefficients, was 0.23°, and the calculated deflection of the nominal center of pressure is 0.29 cm. For approximately 90 percent of the test points the deflections were less than half these values.

Test Procedure

The range of model pitch angles for this test was 20° to 50°. This was obtained by mounting a 10° bent sting onto a 45° strut adaptor to obtain an overall rotation of 35°, thus transforming the tunnel sting mount pitch range of $\pm15^\circ$ to 20° to 50°. To perform the check loading of the main balance, panel balances, and canard pitch angles, the model was first mounted in the tunnel without the 45° strut adaptor so that it could be placed in a level attitute for hanging weights. To eliminate any possibility of wiring mistakes after check loading, the model was then remounted onto the final strut-sting arrangement without disconnecting any of the balance wires. Standard wind tunnel procedures were used for nulling the balances and using calibration resistors. All the model wiring was fastened into grooves in the sting in the rear afterbody region and a fouling strip placed over the wires. Panel balance check loading was performed with the panel covers in place. There was never any indication of fouling during the test program.

Table II lists the conditions for each run of the test program. For comparison purposes with the 6- by 6-Foot Wind Tunnel test previously mentioned, the body-tail configuration was tested at Mach numbers of 0.8 and 1.22, and the other three configurations (body, body-canards, and body - canards-tails) were tested at 0.8 and 1.3.

For this last configuration four combinations of canard deflections 0, 5, 10, and 15 degrees, were tested at the five roll angles and two Mach numbers for the primary test Reynolds number per meter of 6.9×10^6 (2.1×10^6 per foot). A limited amount of testing was also performed at the unit Reynolds numbers of 3.9, 9.5, and 13.5×10^6 per meter (1.2, 3.9, and 4.1×10^6 per foot). This smallest value is the same as was used for all the previous 6- by 6-Foot Wind Tunnel test, so direct comparisons could be made between some of the results. At each run condition data were obtained at each of the following nominal pitch angles: 20°, 22°, 24°, 27°, 30°, 33°, 36°, 39°, 42°, 45°, 48°, and 50°.

To obtain vapor screen flow visualization the tunnel was only partially purged of water vapor to a specific humidity between 0.0004 and 0.0006, as measured by the tunnel humidity gage. The light slit previously described was located on the left side of the tunnel (looking upstream). It made the vortices readily visible to observers outside the wind tunnel. For photography, the light slit was rolled along its track, stopping for about 20 seconds to illuminate each of seven different stations which were marked by white dots on the blackened missile, as indicated in figure 1. The motion picture camera, mounted to the top of the 45° strut (fig. 4), was started and filmed each sweep of the light slit from stations 1 to 7. Double X film was used with a filming speed of 2.8 frames per second. To visualize the flow in the regions within the shadow, either the light source or the model was translated vertically and another sweep was filmed. Sweeps were made at pitch angles of 20°, 24°, 30°, 36°, 42°, and 48°. Numerous difficulties with the photography limited the number of runs for which useful results were obtained to Runs 94 to 97.

DEFINITION OF AERODYNAMIC COEFFICIENTS

All main balance coefficients and panel load summations were calculated in an unrolled body axis system. Note (fig. 8) that the canard and tail panels are both numbered in the counter clockwise direction looking upstream (tails 2 and 4 are switched from this convention in references 1 and 2).

Main Balance and Individual Panel Coefficients

The main balance coefficients, C_N, C_m, C_Y, C_n, C_ℓ, and C_A and the individual panel-balance coefficients, $C_{N_{C_j,T_j}}$, $C_{BM_{C_j,T_j}}$, and $C_{HM_{C_j,T_j}}$ are defined in the conventional manner (see List of Symbols). The moment center of the model is missile station 26 (see List of Symbols, and figs. 1, 8-10).

The rolling-moment coefficient for each panel is defined as follows:

$$C_{RM_{C_j,T_j}} = \left(C_{BM_{C_j,T_j}} + C_{N_{C_j,T_j}} \cdot \frac{a}{\ell_{ref}} \right) \cdot \cos \delta_j \qquad (1)$$

Note that $\delta_j = 0$ for the tail panels for all tests.

Coefficients for Canard Panels Taken Together

For the canard panels taken together, the following aerodynamic coefficients were calculated in an unrolled body axis system:

Normal-force coefficient

$$C_{N_{C(B)}} = C_{N_{C_1}} \cdot \cos \delta_1 \cdot \sin \phi + C_{N_{C_2}} \cdot \cos \delta_2 \cdot \cos \phi + C_{N_{C_3}} \cdot \cos \delta_3 \cdot \sin \phi + C_{N_{C_4}} \cdot \cos \delta_4 \cdot \cos \phi \qquad (2)$$

Side-force coefficient

$$C_{Y_{C(B)}} = -C_{N_{C_1}} \cdot \cos \delta_1 \cdot \cos \phi + C_{N_{C_2}} \cdot \cos \delta_2 \cdot \sin \phi - C_{N_{C_3}} \cdot \cos \delta_3 \cdot \cos \phi + C_{N_{C_4}} \cdot \cos \delta_4 \cdot \sin \phi \qquad (3)$$

Pitching-moment coefficient

$$C_{m_{C(B)}} = \left(\frac{b_c}{\ell_{ref}}\right) \cdot C_{N_{C(B)}} + (C_{HM_{C_2}} + C_{HM_{C_4}}) \cdot \cos\phi + (C_{HM_{C_1}} + C_{HM_{C_3}}) \cdot \sin\phi$$
$$+ (C_{BM_{C_1}} \cdot \sin\delta_1 - C_{BM_{C_3}} \cdot \sin\delta_3) \cdot \cos\phi$$
$$+ (C_{BM_{C_2}} \cdot \sin\delta_2 - C_{BM_{C_4}} \cdot \sin\delta_4) \cdot \sin\phi \qquad (4)$$

Yawing-moment coefficient

$$C_{n_{C(B)}} = \left(\frac{b_c}{\ell_{ref}}\right) \cdot C_{Y_{C(B)}} + (C_{HM_{C_2}} + C_{HM_{C_4}}) \cdot \sin\phi - (C_{HM_{C_1}} + C_{HM_{C_3}}) \cdot \cos\phi$$
$$+ (C_{BM_{C_1}} \cdot \sin\delta_1 - C_{BM_{C_3}} \cdot \sin\delta_3) \cdot \sin\phi$$
$$- (C_{BM_{C_2}} \cdot \sin\delta_2 - C_{BM_{C_4}} \cdot \sin\delta_4) \cdot \cos\phi \qquad (5)$$

Rolling-moment coefficient

$$C_{\ell_{C(B)}} = -C_{RM_{C_1}} + C_{RM_{C_2}} + C_{RM_{C_3}} - C_{RM_{C_4}} \qquad (6)$$

Coefficients for Tail Panels Taken Together

For the tail panels taken together, the following aerodynamic coefficients were calculated in an unrolled body axis system:

Normal-force coefficient

$$C_{N_{T(B)}} = (C_{N_{T_1}} + C_{N_{T_3}}) \cdot \sin\phi + (C_{N_{T_2}} + C_{N_{T_4}}) \cdot \cos\phi \qquad (7)$$

Side-force coefficient

$$C_{Y_{T(B)}} = -(C_{N_{T_1}} + C_{N_{T_3}}) \cdot \cos\phi + (C_{N_{T_2}} + C_{N_{T_4}}) \cdot \sin\phi \qquad (8)$$

Pitching-moment coefficient

$$C_{m_{T(B)}} = -\left(\frac{b_T}{\ell_{ref}}\right) \cdot C_{N_{T(B)}} + (C_{HM_{T_2}} + C_{HM_{T_4}}) \cdot \cos\phi + (C_{HM_{T_1}} + C_{HM_{T_3}}) \cdot \sin\phi \quad (9)$$

Yawing-moment coefficient

$$C_{n_{T(B)}} = -\left(\frac{b_T}{\ell_{ref}}\right) \cdot C_{Y_{T(B)}} + (C_{HM_{T_2}} + C_{HM_{T_4}}) \cdot \sin\phi - (C_{HM_{T_1}} + C_{HM_{T_3}}) \cdot \cos\phi \quad (10)$$

Rolling-moment coefficient

$$C_{\ell_{T(B)}} = -C_{RM_{T_1}} + C_{RM_{T_2}} + C_{RM_{T_3}} - C_{RM_{T_4}} \quad (11)$$

Coefficients for Canard and Tail Panels Taken Together

For the canard panels and tail panels taken together, the following coefficients were calculated in an unrolled body axis system:

Normal-force coefficient: $$C_{N_{C(B)+T(B)}} = C_{N_{C(B)}} + C_{N_{T(B)}} \quad (12)$$

Side-force Coefficient: $$C_{Y_{C(B)+T(B)}} = C_{Y_{C(B)}} + C_{Y_{T(B)}} \quad (13)$$

Pitching-moment coefficient: $$C_{m_{C(B)+T(B)}} = C_{m_{C(B)}} + C_{m_{T(B)}} \quad (14)$$

Yawing-moment coefficient: $$C_{n_{C(B)+T(B)}} = C_{n_{C(B)}} + C_{n_{T(B)}} \quad (15)$$

Rolling-moment coefficient: $$C_{\ell_{C(B)+T(B)}} = C_{\ell_{C(B)}} + C_{\ell_{T(B)}} \quad (16)$$

TEST RESULTS AND DISCUSSION

Presentation of the Data

The run schedule is presented in Table II. Table III is a sample computer sheet showing the data format. The configurations noted there are coded as: 1, body; 2, body-tail; 3, body-canard; and 4, body-canard-tail.

Starting with Run 25 the position potentiometer for canard 3 malfunctioned for the 15° setting and it was positioned manually to $\pm 1/2^{\circ}$ before the start of each set of runs*.

The extensive results of this test are presented elsewhere in the form of DATAMAN plots (ref. 3). Table IV is a list of the figure titles and dependent and independent variables in that report. Figures 11 to 39 are included here to indicate some of the phenomena that were observed. These figures are discussed below.

The body force and moment coefficients and coefficients based on summed panel loads were examined for all non-vapor screen runs for maximum panel loads for the body-tail and body-canard-tail models. Under each value in Table V is a code for identifying the data point. The letters and numbers indicate, from left to right:

α: 20, 22, 24, 27, 30, 33, 35-36, 39, 42, 45, 48, 50°
L K J I H G F E D C B A

M: .8, 1.22, 1.3 $\quad$ $Re.10^{-6}$: 3.9, 6.9, 9.5, 13.5 per meter
X Y Z $\quad$ A B C D

ϕ: 0, 10, 20, 30, 45° $\quad$ $\delta_{1,3}$: 0, 15° $\quad$ $\delta_{2,4}$: 0, 15°
0 1 2 3 4 $\quad$ A B $\quad$ A B

For example, from Table V the maximum C_n for the body-canard-tail configuration is 3.5. This value occurs at GZB1AA, so $\alpha = 33^{\circ}$, M = 1.3, $Re = 6.9 \cdot 10^{6}$, $\phi = 10^{\circ}$, $\delta_{1,3} = 0^{\circ}$, $\delta_{2,4} = 0^{\circ}$.

---

*Run 25 has an erroneous setting for this canard, and it was replaced by Run 26. Starting with Run 38, canard 3 deflection was set on a thumb wheel. For runs between 26 and 37, the 15° setting should be considered accurate, $\pm 1/2^{\circ}$, in spite of an indicated value of $15^{\circ} \pm 2^{\circ}$.

Vapor screen photography was performed for several test conditions at $M = 1.3$ for the body-canard-tail model. The flow visualization quality to the observer appeared to be excellent, however, the resulting film recording is of poor quality, though readable. The coordinate transformations were formulated and the vortex positions determined for one test condition, a roll angle of 20°, canards 1 and 3 at 15° and pitch angle of 20°. More useful than the results from this particular case are the following visual observations for the entire sweep in pitch of the symmetric case (0° roll angle and 0° canard deflections).

$\alpha_c = 20^{\circ}$ "Afterbody vortices appear to start about midway between the fins. At the leading edge of the tail they were about 1.5 radii above the body centerline.

$\alpha_c = 24^{\circ}$ "The phenomena are about the same except body vorticity appears to roll up right after the canards.

$\alpha_c = 30^{\circ}$ "Nose vortices and trailing edge wake of the canards are clearly visible immediately behind the canards. Two calibers later the nose vortices are swept into the canard wake. At the leading edge of the tails the afterbody vortices are unsymmetrical and quite elongated in the Z direction. The left vortex (looking forward) is further from the body than the right vortex.

$\alpha_c = 36^{\circ}$ "There are strong nose vortices at the leading edge of the top canard. These vortices are absorbed into the canard and afterbody wake. The afterbody vortices are symmetrical, strong, and very elongated.

$\alpha_c = 42^{\circ}$ "The behavior is the same, the flow is quite steady.

$\alpha_c = 48^{\circ}$ "As α_c increased the canard wake has become progressively thicker. The wake has become more and more elongated (note that the light planes are vertical, not perpendicular to the body, thus accentuating the vertical stretching of the vortices). The top of the elongated pattern appears to be more distinct and probably consists of the canard vortices. The flow is steady."

Data Accuracy, Repeatability, and Comparison with 6- by 6-Foot Wind Tunnel Test Results

We first examine the data for possible errors accrued in the course of the test. It is convenient to divide the error into two types: sensing and recording errors at the initiation of the test; and errors caused by changing conditions, such as changing calibrations, tunnel conditions, and model conditions. Model check loading was used to examine the first type of error. The main balance accuracy was found to be 0.2 percent of full scale. A comprehensive set of sample panel check loads are presented in Table 1. The percentage standard deviation between actual and recorded loads obtained from a more complete list of check loads was 1.0 percent for panel normal forces and hinge moments, and 1.7 percent for the bending moments on both canards and tails.

An indication of the second type of error is obtained by comparing results from repeat runs, by comparing results with those from previous 6- by 6-wind tunnel test, and by analyzing apparent differences. Those are discussed below.

Figure 11 shows the tail no. 2 normal force and missile side force coefficients for the body-canard-tail model for run 39 and repeat run 77. These curves are typical of the repeatability of the data. The standard deviation of the percentage change in main balance loads from run 39 to run 77 is four percent. The differences are typically only one-third as great for pitch angles between 20° and 33° as compared to the larger pitch angles. The reason for these relatively large differences is unknown, however, there were a moderate number of screw holes and joints that were waxed, and then frequently touched up as the wax occasionally deformed. The main balance loads for a repeat run with the body-only configuration gave much better agreement than the above case.

For the panel loads the standard deviation of the percentage change between runs 39 and 77 is about two percent (excluding the tail no. 1 coefficient CPXT) and there is only a slightly less deviation in values in the lower pitch range as compared to the higher values of pitch. The tail coefficient CPXT is obtained by dividing the hinge moment by the normal force. When the latter becomes very small large errors in CPXT are encountered. These data points are easily identified in the DATAMAN plots by their large scatter; (also, the tail normal force is plotted and its magnitude can be checked).

A phenomenon that frequently occurs in high angle missile model data is vortex switching between two stable configurations. This phenomena has not been observed in the data. Figures 12-18 and 23-26 show data for the body-tail and body-canard-tail models, respectively, at the various test conditions for both the 6- by 6-Foot and 11-Foot Wind Tunnel tests. These data overlap between 20° and 24° pitch. The Reynolds numbers are matched in figures 14, 15, 24, 25, and 26. The comparison is generally quite good. Side force coefficients match up within 0.15, which is 1 or 2 percent of C_N, and yawing moments agree to within 10 percent of the pitching moment.

The difference between the panel coefficients for the 6- by 6-Foot and 11-Foot Wind Tunnel data were examined for twelve different test conditions. The standard deviations of these differences for each panel coefficient were determined to be*:

$\Delta C_{NC} = 0.031$ $\Delta C_{HMC} = 0.004$ $\Delta C_{BMC} = 0.008$

$\Delta C_{NT} = 0.0085$ $\Delta C_{HMT} = 0.020$ $\Delta C_{BMT} = 0.042$

For comparison, these values for the forces are 4.1 and 0.4 percent, respectively, of the maximum values listed in Table V. The bending moments on tails 2, 3, and 4 appear to be significantly larger for the 11-foot than the 6- by 6-foot test, and likewise for the normal force on canard 1. Another possible significant difference is the canard 4 hinge moment, where 11-foot results are considerably less than the 6- by 6-foot test results.

It should be noted that this model at 20° to 24° pitch appeared to create a significant amount of obstruction in the 6- by 6-Foot Wind Tunnel, particularly for the M = 0.8 flow condition. Some tunnel wall effects were probably inevitable for that flow condition. These effects should have been alleviated in the much larger 11-Foot Wind Tunnel.

---

*It has been concluded that the canard hinge moments for the 6- by 6-Foot Wind Tunnel test all have the wrong sign. The listed standard deviation of 0.004 for this coefficient is for the corrected sign.

Phenomena Exhibited by Data

Figures 12 through 39 are presented to indicate some of the phenomena observed. A comprehensive set of DATAMAN plots are included in reference 3. The behavior observed in some of the figures presented here lead to conclusions that have been drawn by examining figures in reference 3. This is indicated by referencing that document. First the figures are considered for the general behavior of the 11-Foot test data, then Reynolds number effects are noted.

The onset of flow asymmetry is best indicated by side force, yawing moment, rolling moment, and normal force on panels in the top vertical position (panel 1). For the body-tail model, flow asymmetry appears to start between 20° and 24° as indicated in figures 12 and 13. The large variations in yawing moment above a pitch angle of 30° (fig. 13) are largely due to the tails in the supersonic case (ref. 3). The model pitching behavior is stable in the subsonic case and only neutrally stable for the supersonic flow case.

Figures 14 and 15 show results for the body-tail model rotated to 20°. The large yawing moments at large pitch angles (fig. 14) are due nearly entirely to the loads on the body (with nose) and not an interaction of nose vortices with the tail panels (ref. 3). For instance, $\alpha = 30^{\circ}$ the yawing moment is -2.64 and the component of this due to the tails is -0.24. Most of this tail yawing moment coefficient is due to normal forces, which are plotted in figure 15. The model has vertical symmetry at both 0° and 45° roll. In figures 16 and 17 it is noted that side forces are considerably less for the 45° roll case than for 0° roll. Maximum side forces occur for 10° and 20° roll.

For the body-canard-tail model at 0° roll, the effect of the canards at 0.80 Mach number is to reduce asymmetries up to a pitch angle of 34°, where yawing moments reach a modest value. Significant asymmetry does not appear until a pitch angle of 48° (fig. 18). As indicated in figure 19 yaw control (canards 1 and 3 deflected) produces a strong side force in the expected direction at lower angles of attack, but the direction of the side force changes sign at about 33°. The larger component of this side force is attributable to the afterbody, as compared to the summed panel loads (ref. 3). Figures 20 to 22 present results for the same case but $M = 1.30$. Pitch control (canards 2 and 4 deflected) decreased side forces and yawing moments. From vapor screen observations (undeflected

canards) previously presented, vortex asymmetry was noted at the tails at only 30° pitch. Yaw control produces an effect similar to the subsonic flow case, that of reversing the sign on the side force and yawing moment. The rolling moments (fig. 22) when yaw control is actuated are due almost entirely to the tail panels (ref. 3). Figure 23 shows selected panel loads. Very little asymmetry in the panel loads is indicated.

Individual panel loads for a roll angle of 20° are indicated in figures 24 to 26. The shadowing effect of the nose and body on canard 1 and tail 1 is evident. This creates a rolling moment which is seen in figure 27. The maximum rolling moment of the test is included in this figure. At the roll angle of 10° the yawing moment is strongly affected by a change from subsonic to supersonic Mach numbers (figs. 28 and 29). The maximum yawing moment for the test occurs in figure 29.

Figures 30 and 31 show four different dependent coefficients, model yawing moment C_n, yawing moment due to the panels CYMB, model rolling moment C_ℓ, and rolling moment due to the panels CRMB, each versus roll angle. These plots conveniently show both the effects of roll angle and the contribution of the appropriately summed components of the panel loads to the total coefficient. Thus, in figure 30 CYMB contributes as much as 1.8 to the largest values of C_n. The total and summed panel load rolling moments, C_ℓ and CRMB, respectively, are shown in figure 31. The only additional source of rolling moment besides CRMB is the tangential component of body skin friction, which is expected to be negligible. Indeed, the pairs of values are within 0.025 except one larger difference of 0.04.

Tests were performed at four different Reynolds numbers. The lowest of these was the same as in the 6- by 6-Foot Wind Tunnel. Not much testing could be performed at that low Reynolds number condition because of extreme conditions placed upon the 11-Foot Wind Tunnel equipment. The changing Reynolds number is not expected to change the flow separation on the panels themselves, but will affect the body boundary layer behavior and thus affect panel loads by changing vortex location near the panels. Figures 15, 24, 25, and 26 show the effects on canards and tails by increasing the Reynolds number by 2.4 and 3.5 times at various test conditions. Figure 15 shows a change in the force on tail 1 of 20 percent of the maximum load and an appreciable effect on tail 2 at 36° pitch angle. Large effects on C_Y and C_n occur for the body tail configuration

corresponding to figure 15 as shown in figures 32 and 33. Figures 34 to 36 exhibit the effect of Reynolds number on the body-canard-tail configuration at a roll angle of 20°. A 10 percent increase in C_N is noted for 3.5 times greater Reynolds number, and a large effect is observed on C_Y (fig. 35).

Vapor screen effects on loads are exhibited in figures 36 to 39. Two positions are included in these curves for the yaw canards. The effect on the panels is small except at maximum loads on tails 2 and 4 (fig. 36) and these differences lead to some rolling moment changes as noted in figure 37. There is an effect on C_N of as much as 5 percent for pitch angles greater than 35°. The panels contribute about half the change to the pitching moment observed in figure 39 (ref. 3).

CONCLUSIONS

A blunt ogive-cylinder missile model with a length-to-diameter ratio of 10.4 has been tested at transonic speeds in the NASA/Ames Research Center Unitary Plan 11-Foot Transonic Wind Tunnel. Four configurations were tested: body, body with tail panels, body with canards, and body with canards and tails. Forces and moments from the entire model and each of the eight fins were measured over the pitch range of 20° to 50° and 0° to 45° roll. Canard deflection angles between 0° and 15° were tested. Exploratory vapor screen flow visualization tests were also made using an 800 watt Xenon lamp to produce a focused light-slit.

Sample force and moment data are reported herein along with observations from the vapor screen tests. Comparisons made of body and panel loads for the same models tested previously in the Ames 6- by 6-Foot Wind Tunnel showed good agreement in the overlapping range of pitch angles of 20° to 24°. For the body-tail model in the symmetric condition the advent of asymmetric flow appeared at 20° to 24°. For the body-canard-tail model at $M = 1.3$ symmetry appeared between 25° and 33°, but was then small for larger pitch angles to 48°, where asymmetric effects became large. Deflecting the canards for pitch control greatly reduced the asymmetry. Canard yaw control produced yawing moments opposite to the direction of the deflection at 20° to 24° at $M = 1.3$.

A Reynolds number range of 3.5:1 (to 13.5 million per meter) was tested for selected conditions. Large effects in side forces and yawing moments were noted for some cases.

REFERENCES

1. Hemsch, M. J. and Nielsen, J. N.: Test Report for Canard Missile Tests in Ames 6- by 6-Foot Supersonic Wind Tunnel. NEAR TR 72, Aug. 1974.
2. Hemsch, M. J. : Reduced Vapor-Screen Data from Canard Missile Tests in Ames 6- by 6-Foot Supersonic Wind Tunnel. NEAR TR 81, Mar. 1975.
3. Allen, C. Q., Schwind, R. G. and Malcolm, G. N.: Canard-Body-Tail Missile Test at Angles of Attack to 50° in the Ames 11-Foot Transonic Wind Tunnel, NASA TM-78,441, 1978.

TABLE I - SAMPLE PANEL CHECK LOAD COMPARISONS

APPLIED LOADS			MEASURED LOADS					
Weight Lbs	Resultg Momt In-Lbs	Momt In-Lbs						
Normal force	Hinge momt	Bending momt	Normal force	Hinge momt	Bending momt	Normal force	Hinge momt	Bending momt
Load at N_1			Canard 1			Canard 3		
+10	+.75	+.58	+9.63	+.76	+.59	+10.05	+.75	+.58
-20	-1.50	-1.16	-19.94	-1.50	-1.16	-20.20	-1.49	-1.15
+50	+3.75	+2.92	+48.14	+3.85	+2.97	+50.07	+3.75	+2.91
-50	-3.75	-2.92	-49.85	-3.75	-2.91	-49.92	-3.75	-2.92
Load at N_2								
+40	0	2.33	+39.47	+.03		+40.13	-.01	+2.33
-50	↓	-2.92	-50.44	+.05	-2.88	-50.60	+.03	-2.89
+100		+5.84	+97.84	+.14		+99.68	+.02	+5.85
-110		6.42	-110.33	+.07	-6.37	-109.74	-.01	-6.42
Load at N_3								
+30	0	+4.50	29.88	0	+4.47	30.09	-.02	+4.50
-40	↓	-6.00	-40.47	.06	-5.95	-40.79	+.04	-5.99
+80		+12.00	78.62	+.09	+11.97	79.78	+.01	+12.02
-80		-12.00	-80.55	+.08	-11.92	-79.80	-.01	-12.00
Load at N_1			Tail 2			Tail 3		
+70	-5.833	+9.32	70.19	-5.74	+9.47	69.22	-5.85	9.45
-70	+5.833	-9.32	-70.68	5.67	-9.34	-68.97	+5.81	-9.32
+140	-11.67	+18.64	140.76	-11.39	+18.94	139.06	-11.58	18.89
-140	+11.67	-18.64	-141.6	11.28	-18.60	-138.25	+11.59	-18.63
Load at N_2			Load					
+70	+5.833	+9.32	69.57	+5.77	9.47	69.26	+5.68	9.39
-70	-5.833	-9.32	-69.79	-5.82	-9.34	-69.18	-5.76	-9.29
+140	+11.67	+18.64	139.38	+11.51	18.91	138.81	+11.41	18.75
-140	-11.67	-18.64	139.80	-11.64	-18.56	-138.51	-11.53	-18.60
Load at N_3								
50	0	+10.83	49.91	+.04	+10.91	49.33	-.03	10.90
-50	↓	-10.83	-50.09	-.06	-10.82	-49.51	-.01	10.80
100		+21.65	99.88	+.09	21.83	98.91	-.03	21.77
-100		-21.65	-100.20	-.13	-21.62			

TABLE II.- RUN SCHEDULE

Configuration	Roll ϕ	P_T psf	Re/ft $\times 10^{-6}$	Canard δ's		Run number at Mach number			Vapor run specific humidity
				1 & 3	2 & 4	0.8	1.22	1.3	
1 (Body)	0	1008	2.1					2	
2 (Body & tails)	0	↓	↓			5	4	3	
↓	30					7	6		
↓	45					9	8		
↓	10					11	10		
↓	20	576	1.2			13	12		
↓	↓	1008	2.1			14	15		
↓	↓	1440	2.9			17	16		
1 (Body)	0	1008	2.1			20	19	18	
↓	0	1440	2.9			21		22	
3 (Body & canards)	0	1008	2.1	0	0	29		23	
↓	0	↓	↓	0	15			24	
↓	0	↓	↓	15	15	27		25	
↓	↓	↓	↓	15	15			26	
↓	↓	↓	↓	15	0	28			
4 (Body & canards & tails)	↓	↓	↓	15	0	33		30	
↓	↓	↓	↓	15	15	32		31	
↓	↓	↓	↓	0	0	34		37	
↓	↓	↓	↓	0	15	35		36	
↓	↓	↓	↓	15	0			38	High

TABLE II.- CONTINUED

Configuration	Roll ϕ	P_T psf	Re/ft $\times 10^{-6}$	Canard δ's		Run number at Mach number			Vapor run specific humidity
				1 & 3	2 & 4	0.8	1.22	1.3	
4 (Body & canards & tails	20	1008	2.1	15	15	41		40	
		1008	2.1	15	0	42		39	
		580	1.2	15	0	43			
		1440	2.9	15	0	44			
		1008	2.1	0	0	45		48	
		1008	2.1	0	15	46		47	
		580	1.2	0	0			49	
		1440	2.9	0	0			50	
	45	1008	2.1	15	15	53		52	
				15	0	54		51	
				0	0	55		58	
				0	15	56		57	
	30			15	0	62		59	
				15	15	61		60	
				0	0	63		66	
				0	15	64		65	
	10			15	0	70		67	
				15	15	69		68	
				0	0	71		74	
				0	15	72		73	

TABLE II.- CONCLUDED

Configuration	Roll ϕ	P_T psf	Re/ft $\times 10^{-6}$	Canard δ's		Run number at Mach number			Vapor run specific humidity
				1 & 3	2 & 4	0.8	1.22	1.3	
4 (Body & canards & tails	20	1008	2.1	15	0			75	0.00055
	↓	1008	2.1	↓	↓			77	
		1440	2.9			79		78	
		580	1.2			80		76	
		2160	4.1	↓		81			
		580	1.2	0		82			
		1440	2.9	↓		83			
	↓	2160	4.1		↓	84			
	0	1008	2.1		5	88		85	
	↓	2160	4.1	↓	5	89			
		1008	2.1	0	10	87		86	
		2160	4.1	0	10	90			
		↓	↓	↓	15	91			
					0	92			
		1008	2.1	15	↓			93	0.00063
	↓	↓	↓	0				94	0.00058
	20			15				95	0.00070
	↓			15				96	0.00039
				0	↓			97	0.00039
↓									

TABLE III.- SAMPLE OF DATA OUTPUT

```
0      RUN SEQ
        49 10
0
     MACH    RN/FT   CONF      PT       P       Q       TTF
     1.29    1.29       4   596.9   219.1   254.3    84.1

    ALPHA   BETA   PHI_M      CN      CS      CA     CPM     CYM     CRM      D1      D2      D3      D4   PHI_C   PHI_T    CPXN    CPXY
    44.96   0.31   20.00  15.005  0.0513  0.4446 -9.6490  0.3452  0.7610   -0.09   -0.07    0.00    0.03   20.00   20.00  5.8430 -1.5282

  CANARDS
    CNC1   CHMC1   CBMC1   CRMC1   CNC2   CHMC2   CBMC2   CRMC2   CNC3   CHMC3   CBMC3   CRMC3   CNC4   CHMC4   CBMC4   CRMC4
 -0.0323 -0.0074  0.0148 -0.0014 0.4779 -0.0312  0.1407  0.3797 0.2190 -0.0023  0.1021  0.2616 0.6831 -0.0359  0.1819  0.5234

  TAILS
    CNT1   CHMT1   CBMT1   CRMT1   CNT2   CHMT2   CBMT2   CRMT2   CNT3   CHMT3   CBMT3   CRMT3   CNT4   CHMT4   CBMT4   CRMT4
  0.0301  0.0141  0.0025  0.0175 0.9634 -0.2451  0.3046  0.7863 0.9852 -0.1505  0.2765  0.7691 1.3136 -0.2044  0.3038  0.9606

  CANARDS TOTAL      CNC      CYC      CMC      CYMC     CRMC          TAILS TOTAL      CNT      CYT      CMT      CYMT     CRMT
                  1.1890   0.1277   2.5489   0.2683  0.119174                       2.3970   0.6858  -10.020  -2.9279  0.577204

  ALL PANELS TOGETHER      CNB      CYB      CMB     CYMB     CRMB
                           3.5860   0.8136  -7.4709  -2.6596  0.696378

  CP CANARDS                                                                CP TAILS
    CPXC1   CPYC1   CPXC2   CPYC2   CPXC3   CPYC3   CPXC4   CPYC4   CPXT1   CPYT1   CPXT2   CPYT2   CPXT3   CPYT3   CPXT4   CPYT4
 -0.2289 -0.4579  0.0453  0.2945  0.0104  0.3199  0.0526  0.2662 -0.4693  0.0817  0.2544  0.3161  0.1527  0.2806  0.1556  0.2313
1TST-183 PH-1 TN-11  49 11          ID-PRESSOUTO          15 DEC 76@03 50          PAGE 574
0      RUN SEQ
        49 11
0
     MACH    RN/FT   CONF      PT       P       Q       TTF
     1.29    1.29       4   597.6   219.8   254.5    83.9

    ALPHA   BETA   PHI_M      CN      CS      CA     CPM     CYM     CRM      D1      D2      D3      D4   PHI_C   PHI_T    CPXN    CPXY
    47.75   0.33   20.00  15.832  0.0002  0.4212 -10.161  0.5393  0.7905   -0.09   -0.07    0.00    0.04   20.00   20.00  5.8418 -2797.2

  CANARDS
    CNC1   CHMC1   CBMC1   CRMC1   CNC2   CHMC2   CBMC2   CRMC2   CNC3   CHMC3   CBMC3   CRMC3   CNC4   CHMC4   CBMC4   CRMC4
 -0.0279 -0.0070  0.0155  0.0019 0.4653 -0.0350  0.1408  0.3734 0.3160 -0.0036  0.1005  0.2585 0.6946 -0.0375  0.1845  0.5318

  TAILS
    CNT1   CHMT1   CBMT1   CRMT1   CNT2   CHMT2   CBMT2   CRMT2   CNT3   CHMT3   CBMT3   CRMT3   CNT4   CHMT4   CBMT4   CRMT4
 -0.0013  0.0140 -0.0062 -0.0069 0.9807 -0.2695  0.3057  0.7958 1.0163 -0.1568  0.2818  0.7899 1.3375 -0.2074  0.3072  0.9760

  CANARDS TOTAL      CNC      CYC      CMC      CYMC     CRMC          TAILS TOTAL      CNT      CYT      CMT      CYMT     CRMT
                  1.1888   0.1254   2.5435   0.2612  0.098183                       2.4279   0.7123  -10.169  -3.0464  0.616619

  ALL PANELS TOGETHER      CNB      CYB      CMB     CYMB     CRMB
                           3.6167   0.8377  -7.6254  -2.7852  0.714802

  CP CANARDS                                                                CP TAILS
    CPXC1   CPYC1   CPXC2   CPYC2   CPXC3   CPYC3   CPXC4   CPYC4   CPXT1   CPYT1   CPXT2   CPYT2   CPXT3   CPYT3   CPXT4   CPYT4
 -0.2504 -0.5695  0.0751  0.3026  0.0113  0.3180  0.0539  0.2656  10.623  4.7200  0.2750  0.3118  0.1543  0.2773  0.1551  0.2297
1TST-183 PH-1 TN-11  49 12          ID-PRESSOUTO          15 DEC 76@03 50          PAGE 575
```

TABLE IV - DATAMAN PLOT TITLES, DEPENDENT AND INDEPENDENT VARIABLES (REF. 3)

TITLE	VALUES PLOTTED ON: Y-AXIS (VARIOUS PLOTS)	X-AXIS
FIG. 1 BODY-ALONE CHARACTERISTICS	CN, CM, CPXN, CY, CYM, CRM	α
FIG. 2 BODY-TAIL CHARACTERISTICS, MAIN BALANCE AND PANEL LOAD SUMMATIONS	CN, CNB, CM, CMB, CY, CYB, CYM, CYMB, CRM, CRMB	α
	DITTO	ϕ
FIG. 3 BODY-CANARD CHARACTERISTICS, MAIN BALANCE AND PANEL LOAD SUMMATIONS	DITTO	α
FIG. 4 BODY-CANARD-TAIL MAIN BALANCE AND TOTAL PANEL LOADS VS PITCH ANGLE	DITTO	α
FIG. 5 BODY-CANARD-TAIL MAIN BALANCE AND TOTAL PANEL LOADS VS ROLL ANGLE	DITTO	ϕ
FIG. 6 BODY-TAIL CHARACTERISTICS, INDIVIDUAL PANEL LOADS AND CENTERS OF PRESSURE	CNT_i, $CBMT_i$, $CPXT_i$, $CPYT_i$, $i = 1, 2, 3, 4$	α
	DITTO	ϕ
FIG. 7 BODY-CANARD CHARACTERISTICS, PANEL LOADS AND CENTERS OF PRESSURE	CNC_i, $CBMC_i$, $CPXC_i$, $CPYC_i$, $i = 1, 2, 3, 4$	α
FIG. 8 BODY-CANARD-TAIL CHARACTERISTICS, PANEL LOADS AND CENTERS OF PRESSURE VS. PITCH ANGLE	ALL COEFFICIENTS IN BOTH FIGS. 6 AND 7	α
FIG. 9 BODY-CANARD-TAIL CHARACTERISTICS, PANEL LOADS AND CENTERS OF PRESSURE VS. ROLL ANGLE	DITTO	ϕ
FIG. 10 BODY-CANARD-TAIL, REYNOLDS NUMBER EFFECTS ON PANELS	DITTO	α
FIG. 11 BODY-CANARD-TAIL, REPEAT RUNS	ALL COEFFICIENTS IN FIGS. 2, 6 AND 7	α
FIG. 12 EFFECT OF VAPOR SCREEN TUNNEL HUMIDITY	DITTO	α

TABLE V - EXTREME VALUES FOR SELECTED COEFFICIENTS*

	Body		Body-Tail		Body-Canard (ϕ = 0)		Body-Canard-Tail	
	min	max	min	max	min	max	min	max
C_N	1.4	12.1	4.2	15.5	2.7	14.0	4.6	17.6
	LXB	AZB	LXB3	AZB0	LXB0AA	AZB0BB	LXA2BA	AZB0AA
C_m	-1.2	5.3	-17.2	-7.0	2.4	9.8	-13.1	-3.2
	AZB	BXC	BZB0	AXB4	BZB0BB	CXB0AA	CZB0AA	LZB4BB
CPXN	3.83	5.30	5.82	7.51	3.35	5.3	5.47	6.46
	LXB	AZB	AXB4	LXB0	LXB0AA	AZB0BB	AXB4BB	LXB0AA
C_Y	-.08	1.49	-.51	2.35	-1.68	.51	-2.1	1.36
	GXB	GXC	AXB3	FXC2	LXB0AB	HZB0AA	LXB0BA	BXB4BB
C_n	-.40	2.45	-3.45	1.0	-3.30	.70	-3.75	3.5
	IXB	FXC	HYB2	AYB3	GXB0BA	DZB0AA	GZB0BB	GZB1AA
C_ℓ		.02	-.16	.89	-.05	.09	-0.33	1.06
		A--	CXB4	FXC2	IXB0BA	AZB0BB	JXB0BA	AXB2AB
CNB			1.30	3.41	.67	1.37	2.44	4.31
			AXB4	CZB0	LXB0AA	AZB--	LXB0B4	CZB0AA
CMB			-14.2	-5.4	1.5	2.9	-9.7	-3.9
			CZB0	AXB4	LXB0AA	AZB0--	CZB0AA	LZB4BB
CYB			-1.86	.24	-.6	.06	-1.08	.40
			CYB4	FYB0	LXB0BA	LXB0AA	KZB0BA	BXB3AB
CYMB			-1.0	7.9	-1.35	.16	-2.4	1.76
			FYB0	CYB4	LXB0BB	FXB0AA	FZB0BB	FZB1AA
CNC1								.50
								LZB4BB
CNC2								.70
								AZB0BB
CNC3								.68
								AZB4BA
CNC4								.75
								AZB1BB
CNT1				.70				.63
				FXB4				FXB4AB
CNT2				1.50				1.46
				DYB0				DZB0AA
CNT3				1.49				1.49
				DYB4				AZB4AB
CNT4				1.56				1.52
				DYB3				AZB4AB

*Second line for each coefficient is the test condition code. It is explained in section 5. Note that the reference area for all coefficients is the body cross section. Individual canard and tail areas are .406 and .936, respectively of the body area.

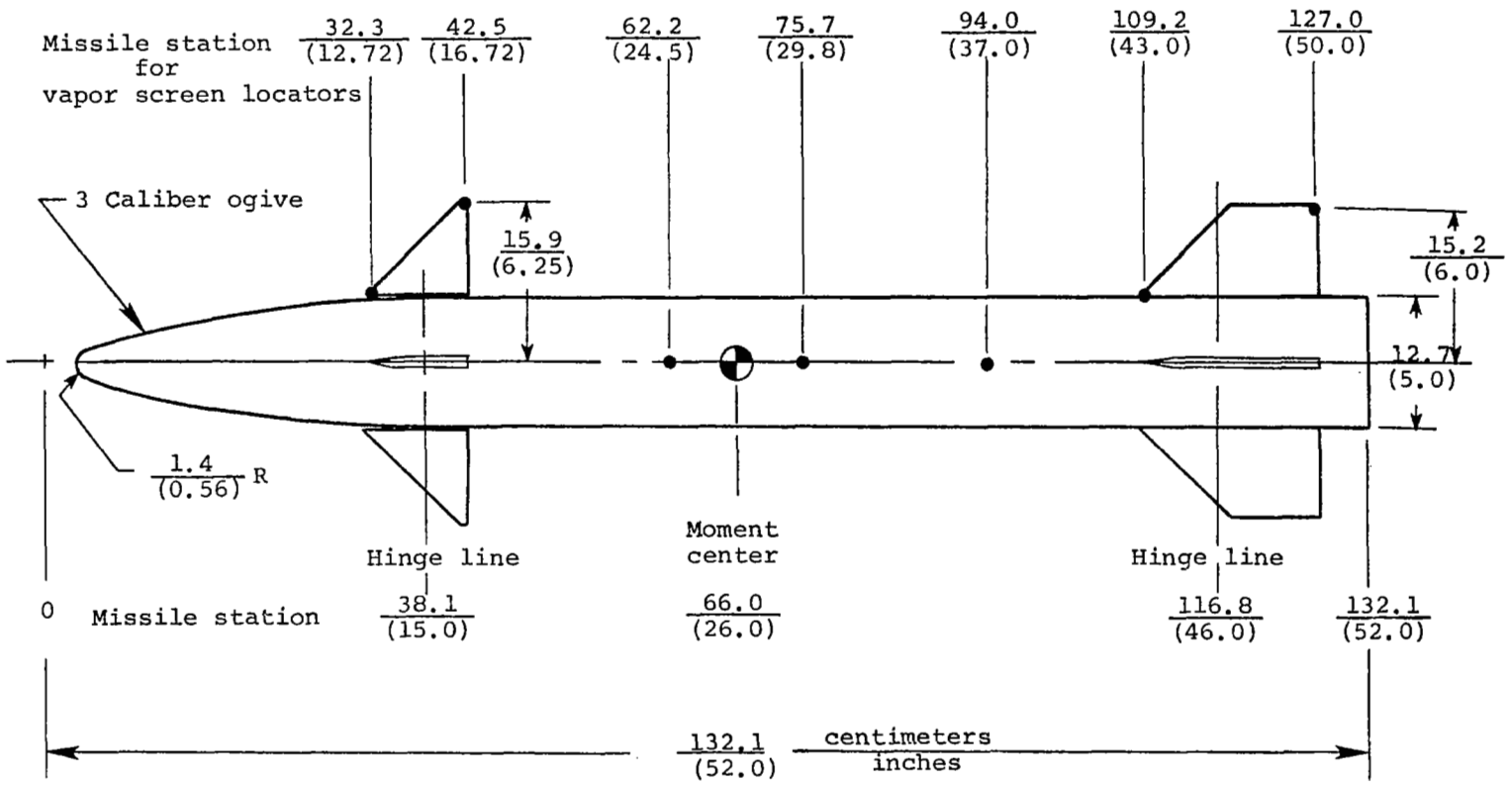

Figure 1.- Body-canard-tail test configuration and vapor screen markers.

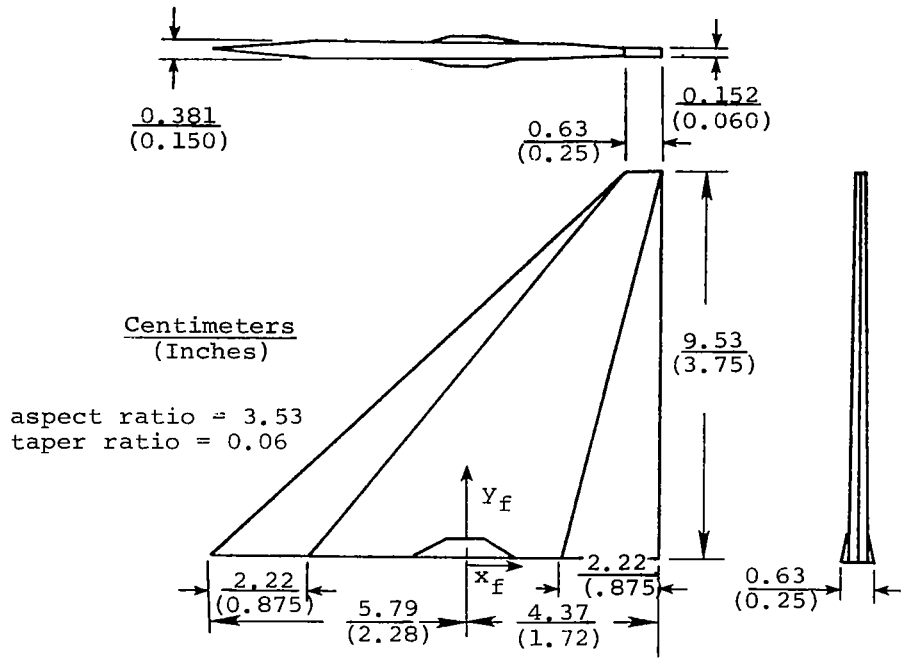

Figure 2.- Canard.

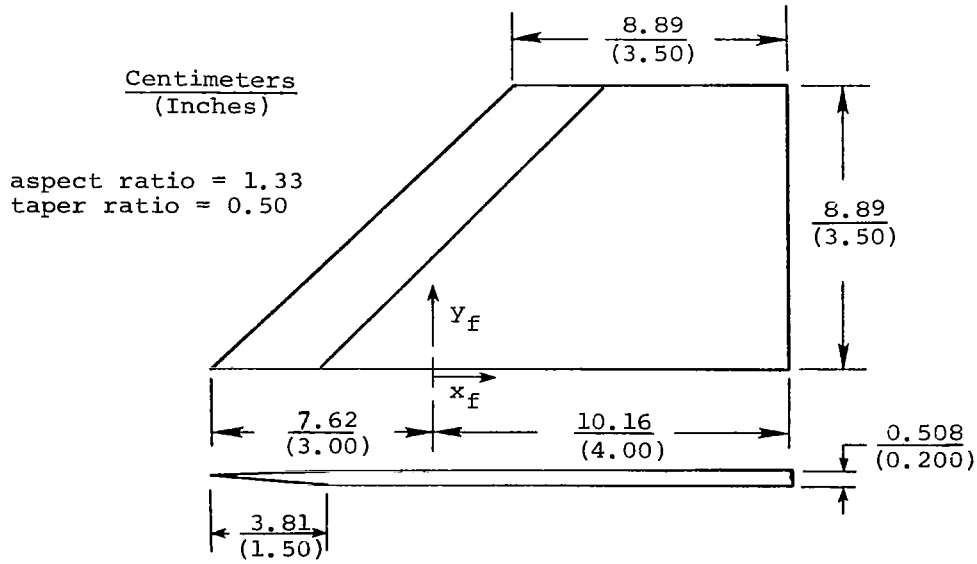

Figure 3.- Tail.

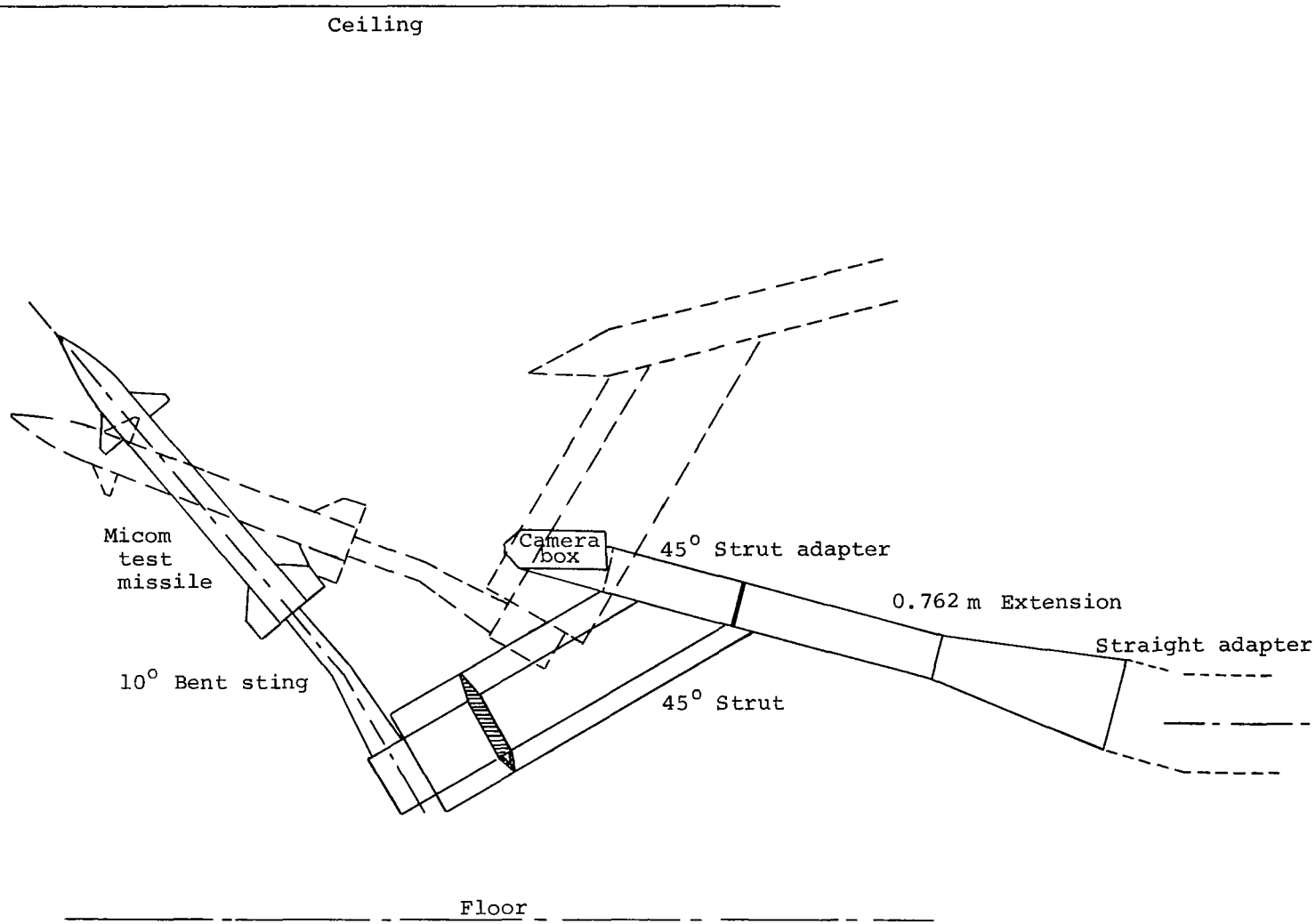

Figure 4.- Model mounting arrangement.

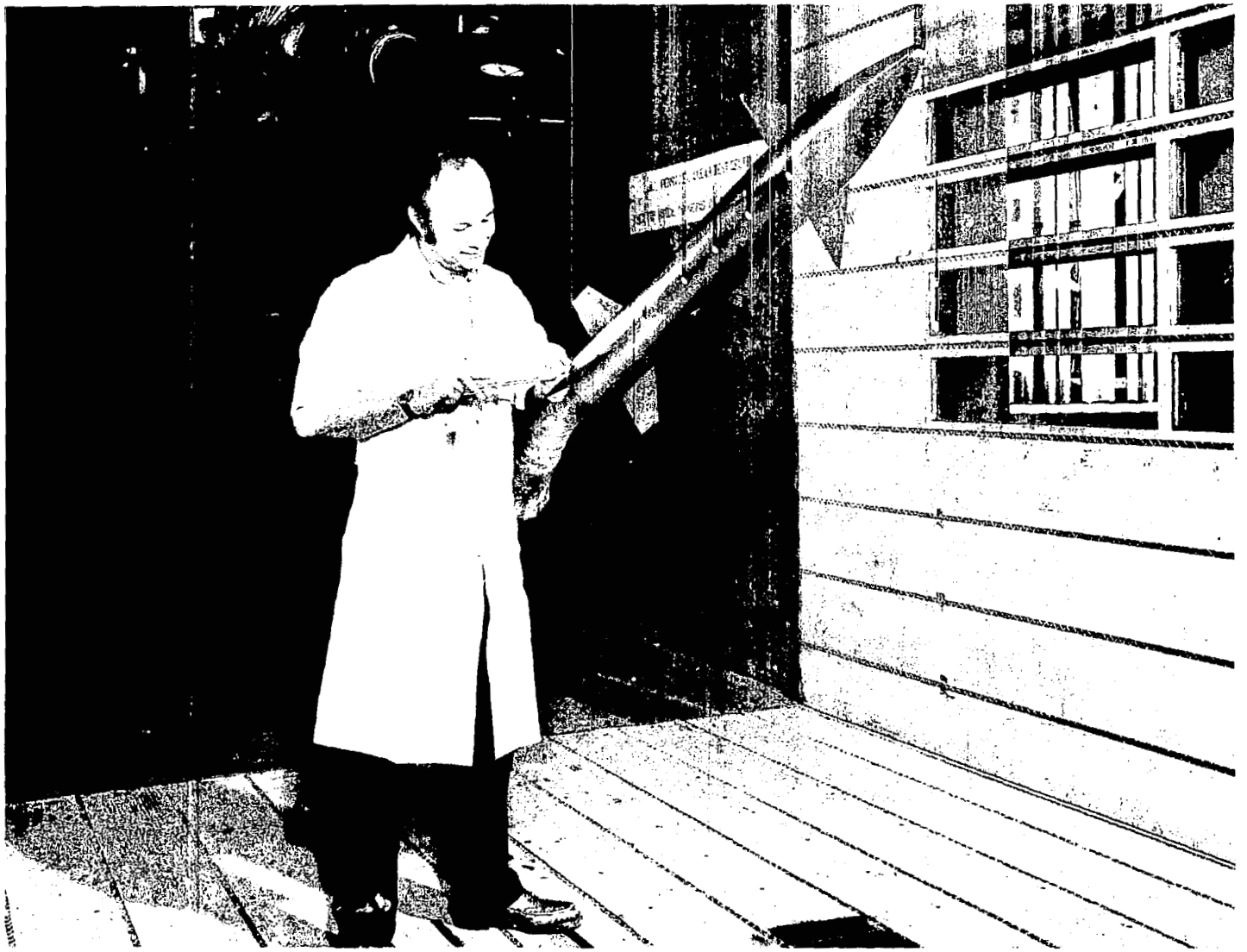

Figure 5.- Model installed in the 11-Foot Wind Tunnel, looking downstream.

Figure 6.- Model installed in the 11-Foot Wind Tunnel, looking upstream.

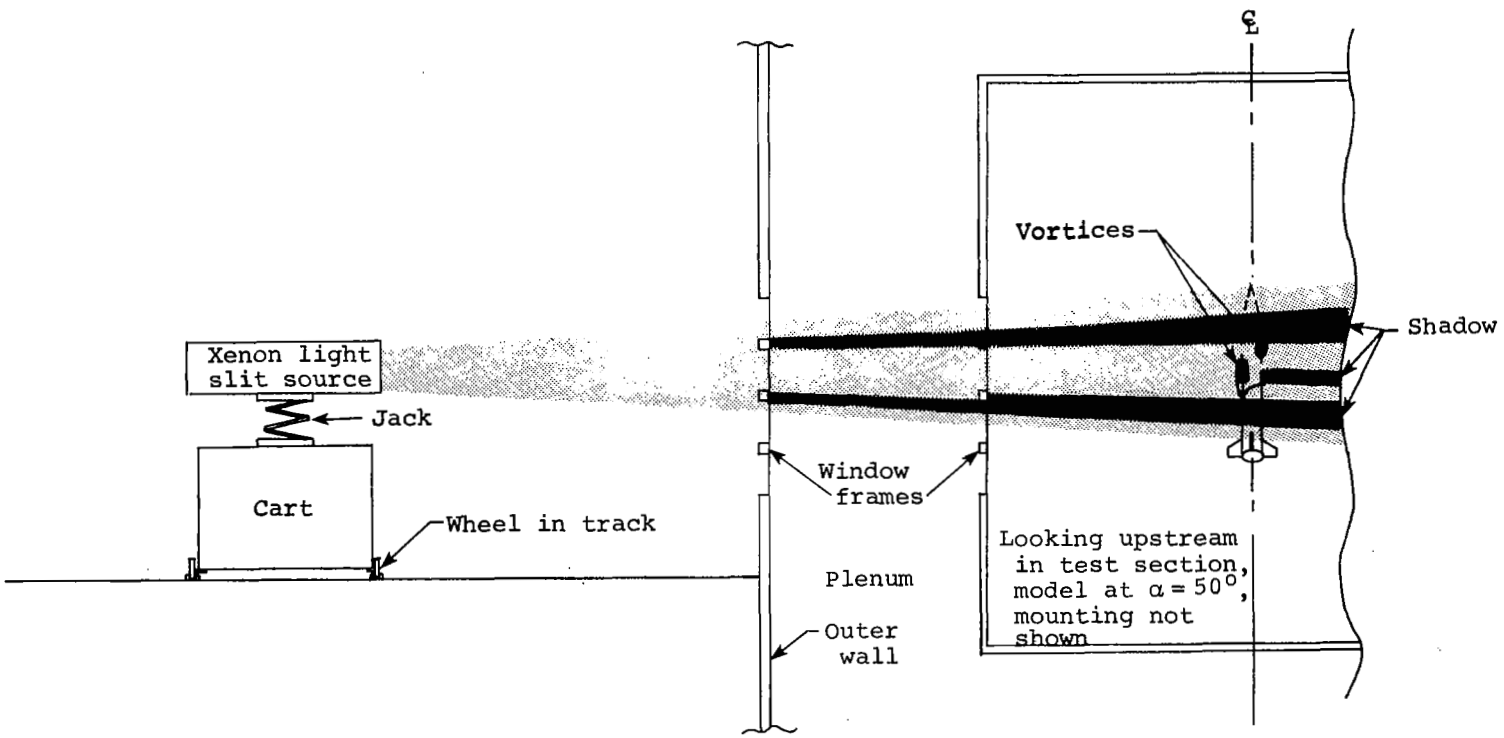

Figure 7.- Vapor screen light slit arrangement, 11-Foot Wind Tunnel.

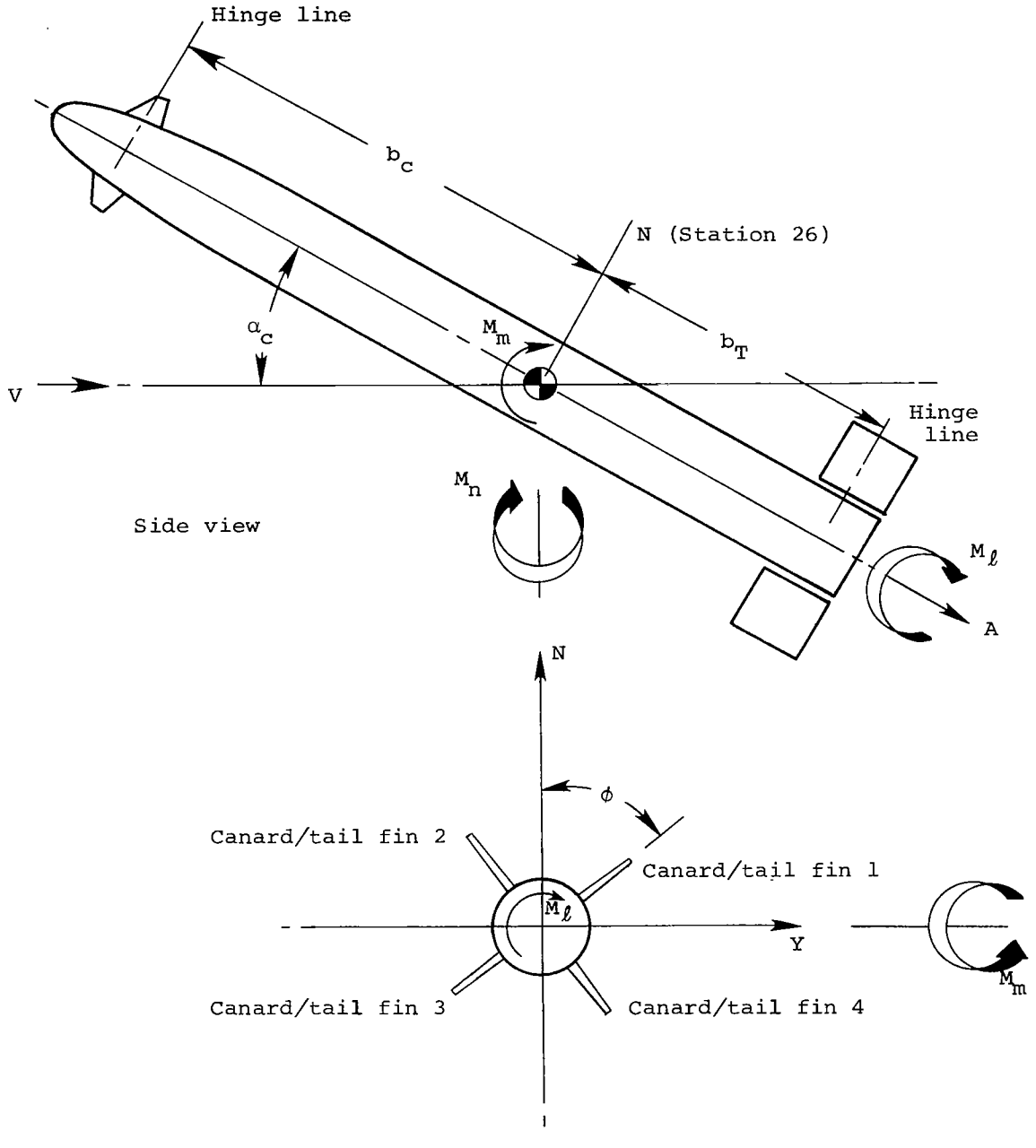

View looking forward

Figure 8.- Axis system and positive sign convention; unrolled body axis system.

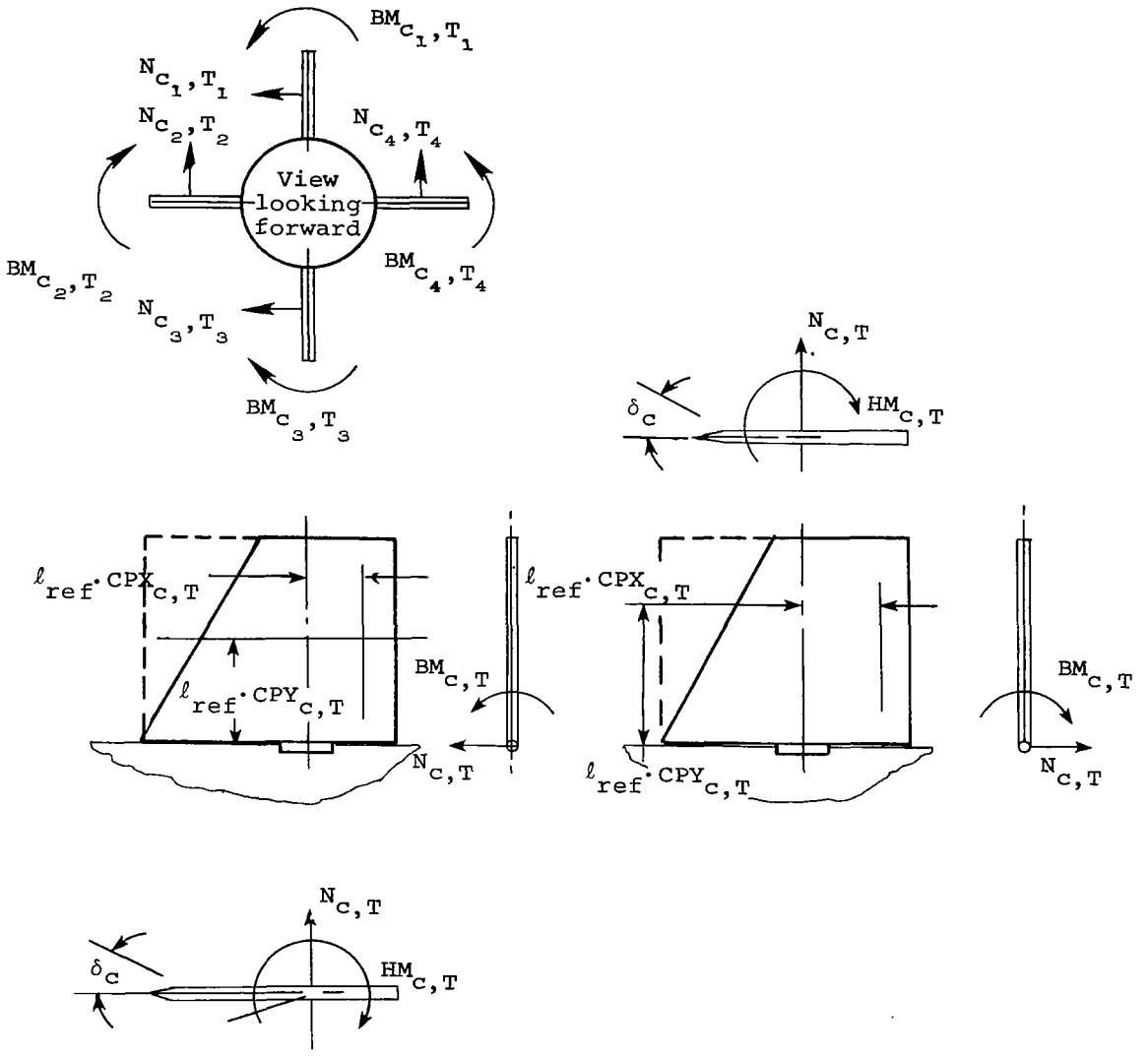

Canards and tails 1 and 4

Canards and tails 2 and 3

Figure 9.- Axis systems and positive sign convention (typical) canards and tail fins. Normal forces are measured perpendicular to the panel planform. Note that both canard and tail panels are numbered counterclockwise.

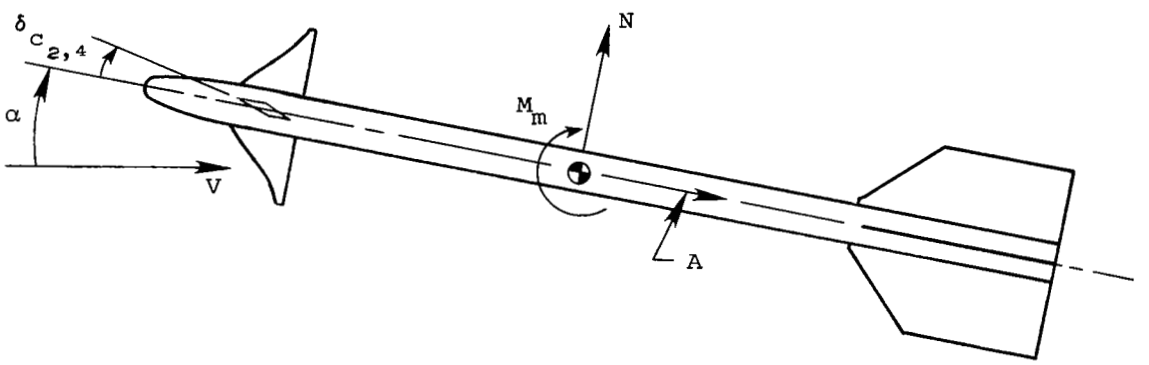

Pitch plane

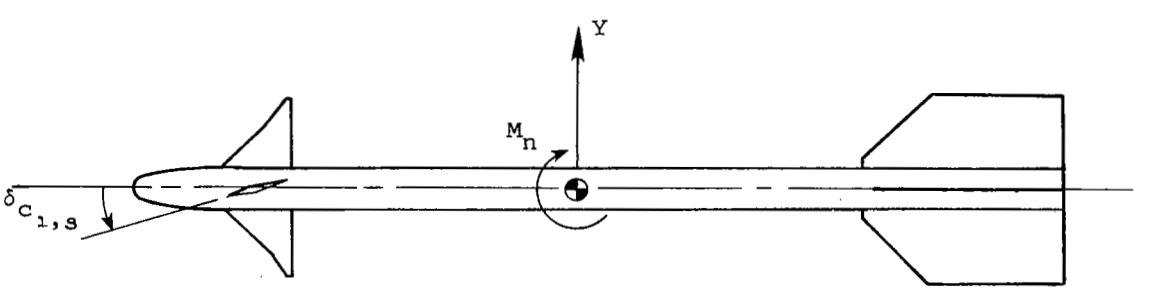

Yaw plane
(Top view)

Figure 10.- Sign convention for canard deflection angles.

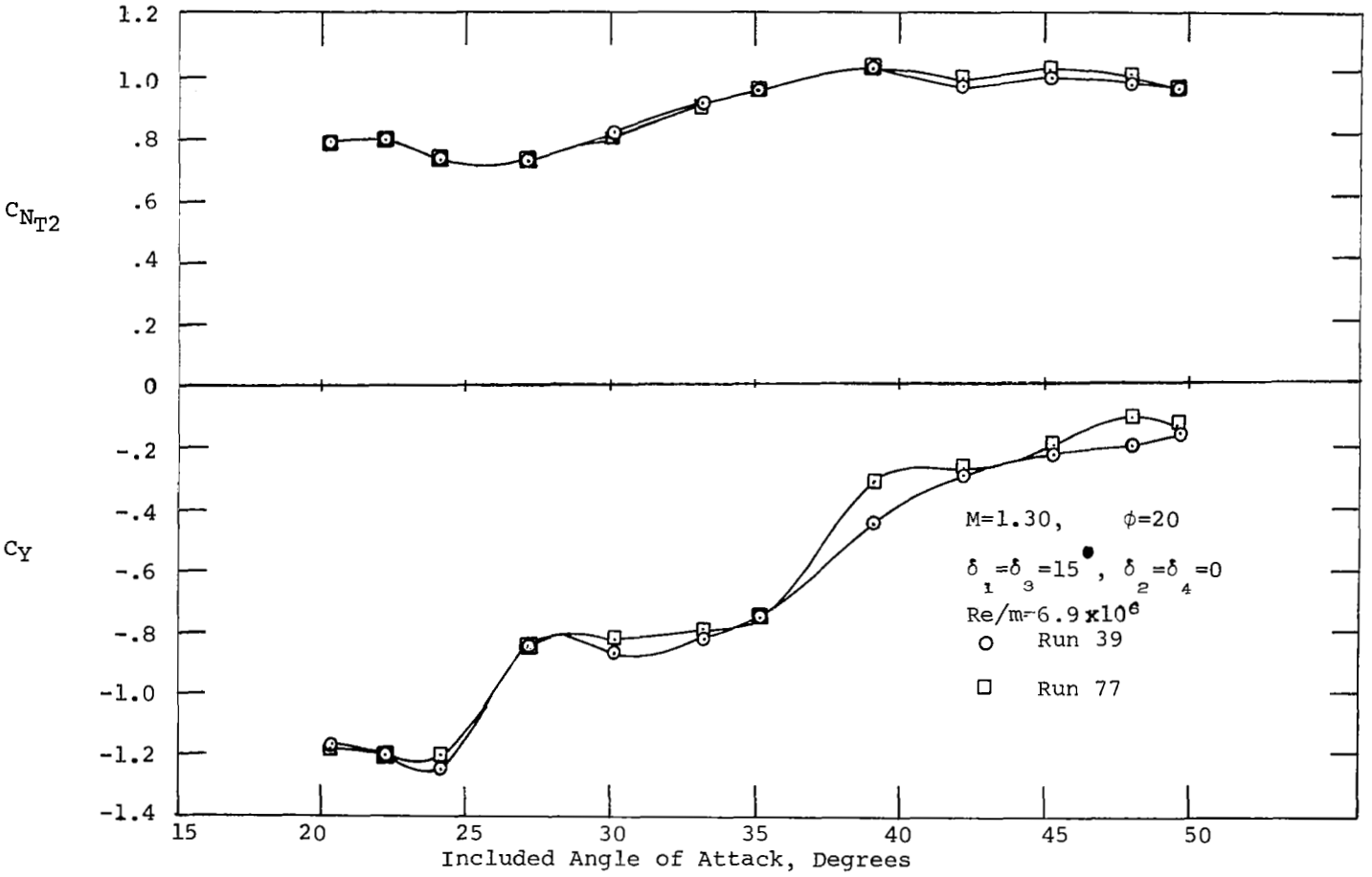

Figure 11 Typical Repeat Run Results, Body-Canard-Tail Model

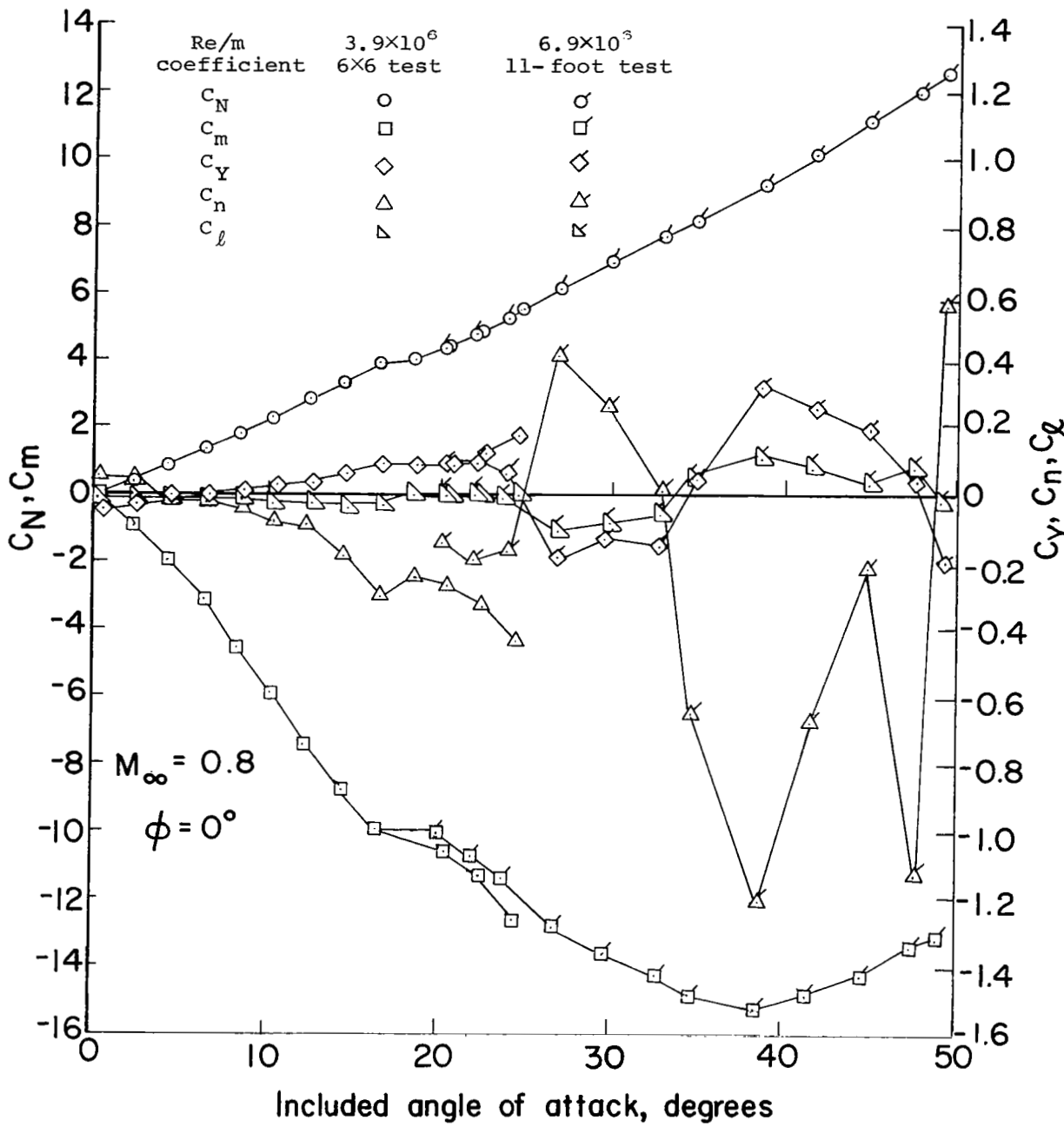

Figure 12.- Comparison of main balance data from 6- by 6- and 11-foot tests at primary test Reynolds numbers. Body-tail model

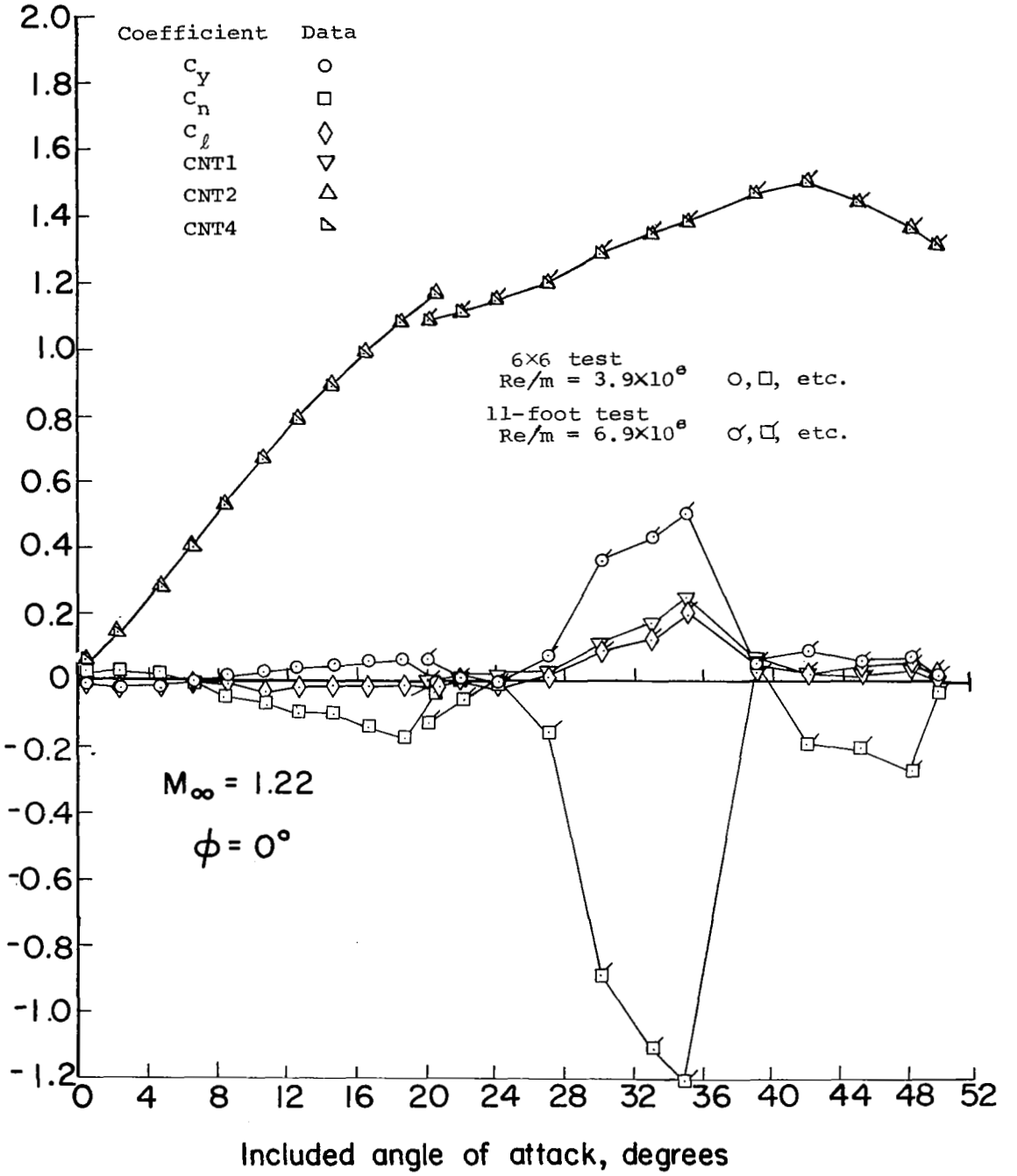

Figure 13.- Comparison of data for 6- by 6- and 11-foot tests for primary test Reynolds numbers showing onset of asymmetry. Body-tail model.

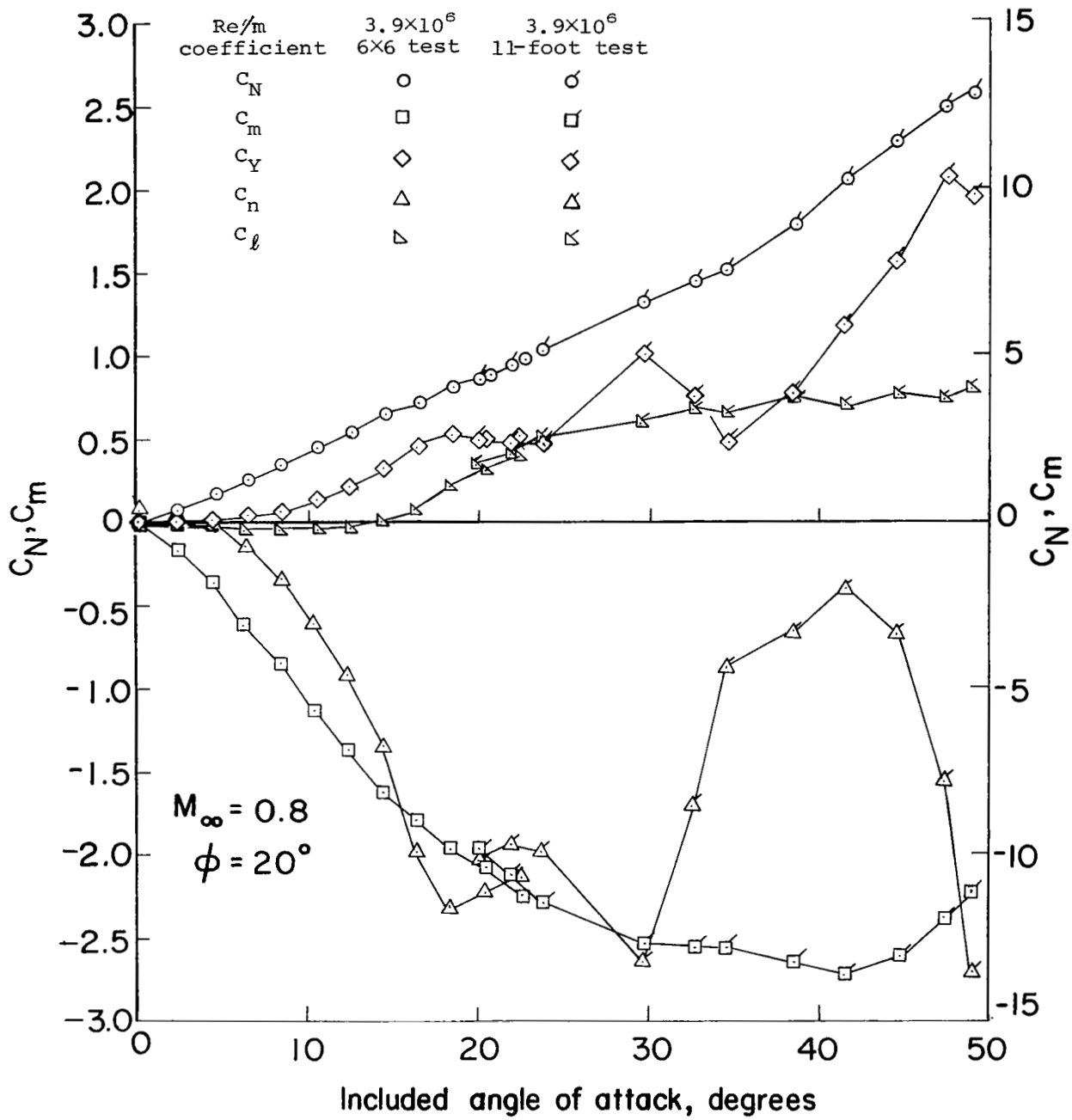

Figure 14.- Comparison of main balance data from 6- by 6- and 11-foot tests at same Reynolds number, body-tail model.

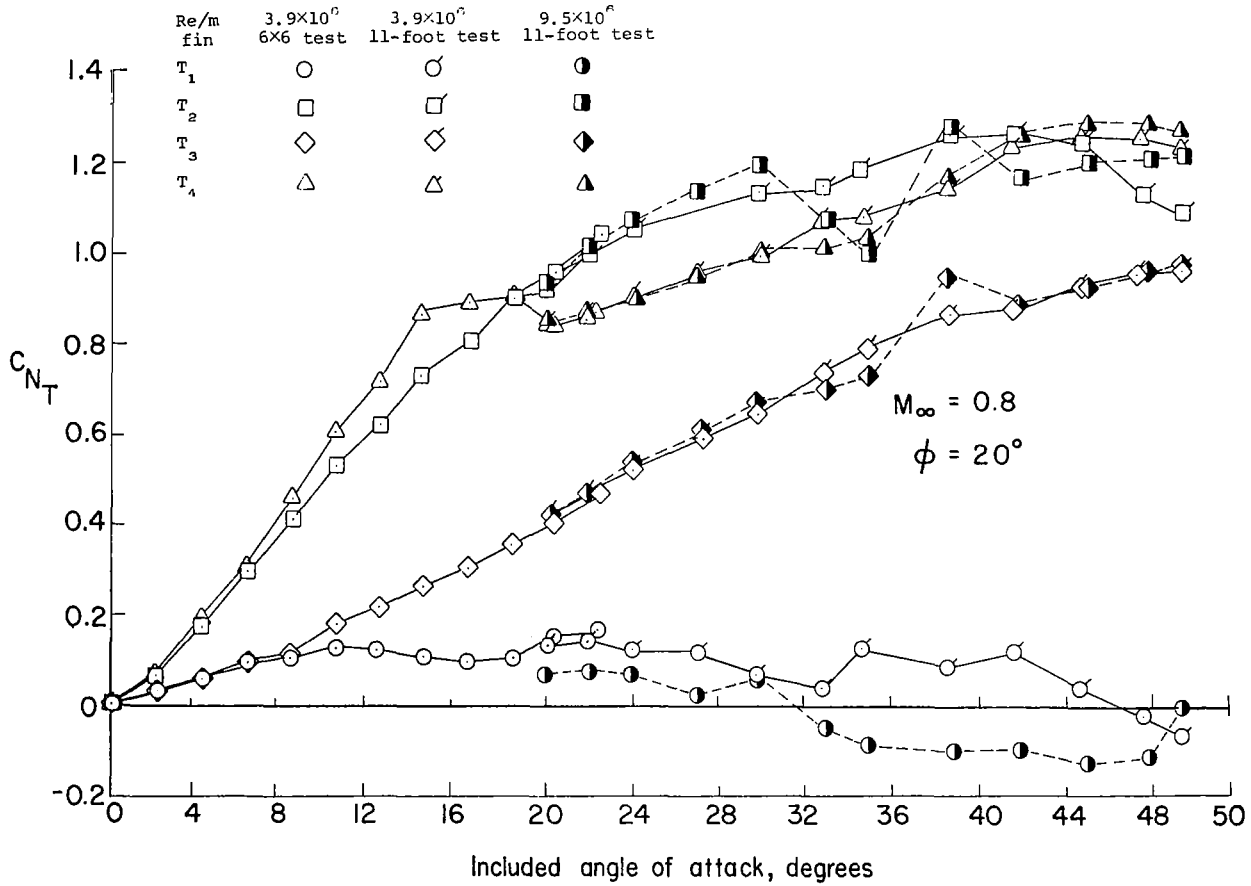

Figure 15.- Comparison of tail fin balance data for 6- by 6- and 11-foot tests for different Reynolds numbers, body-tail model.

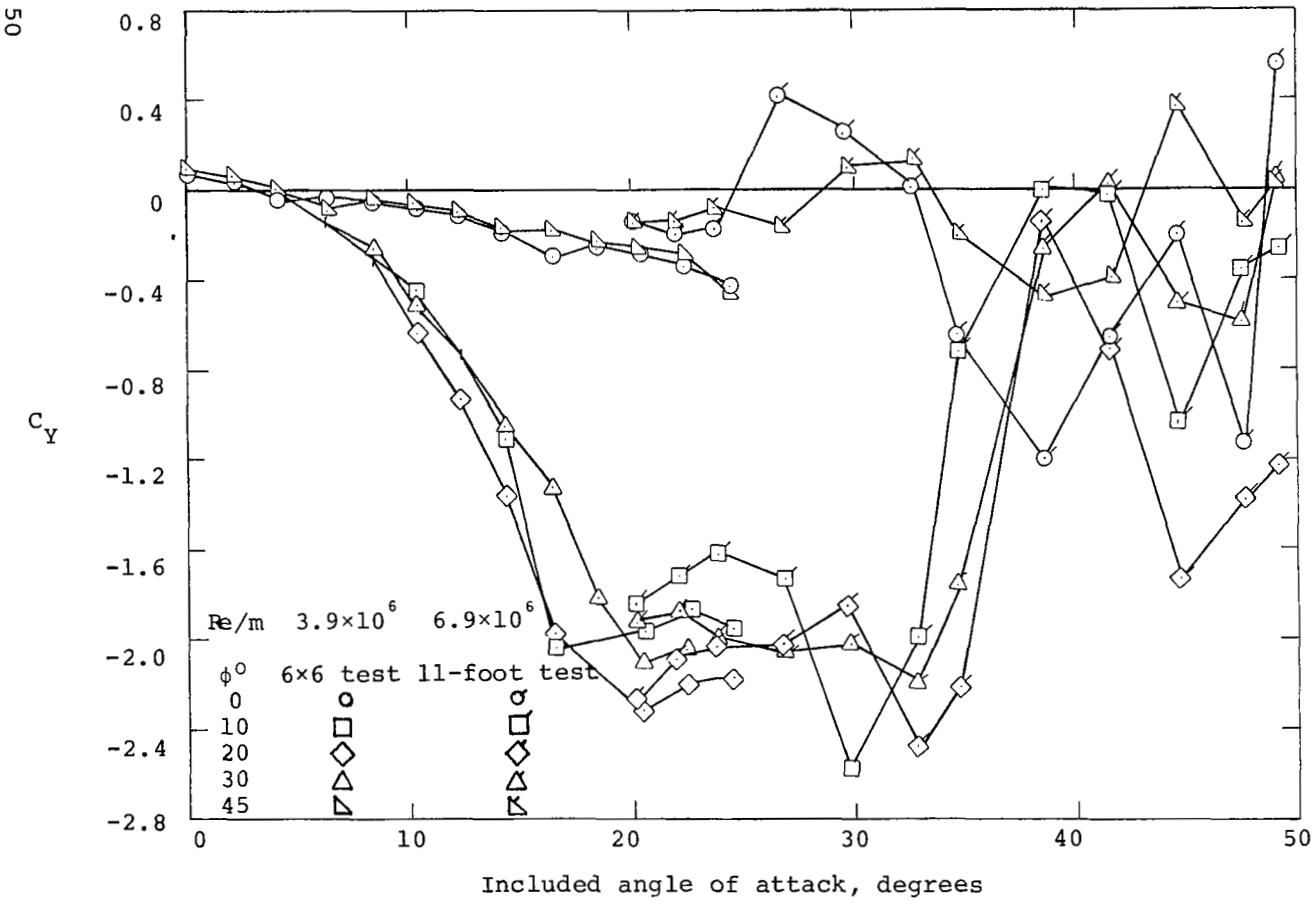

Figure 16.- Comparison of side force for 6- by 6- and 11-foot tests, body-tail model, M = 0.8

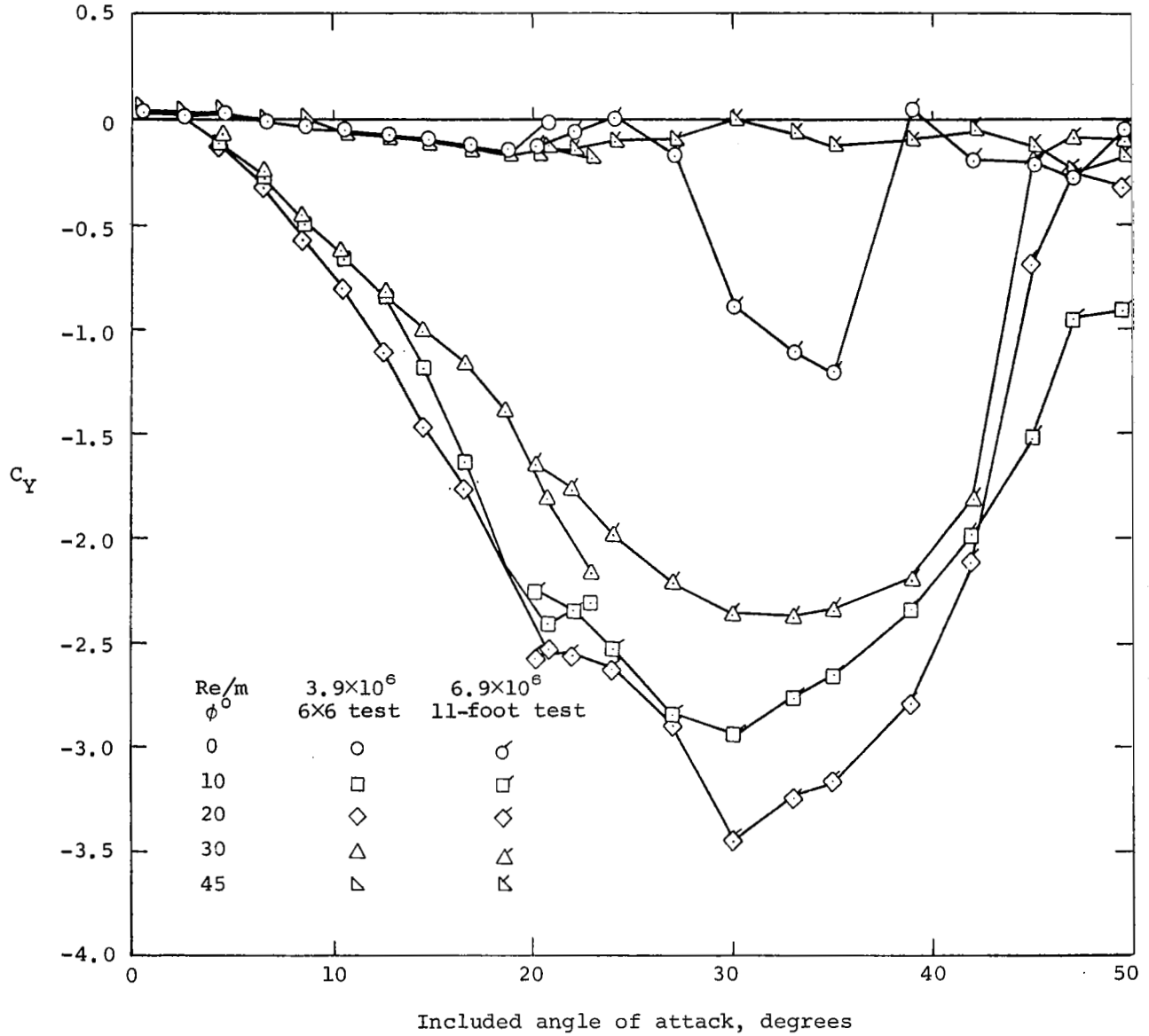

Figure 17.- Comparison of side force for 6- by 6- and 11-foot tests, body-tail, M = 1.22.

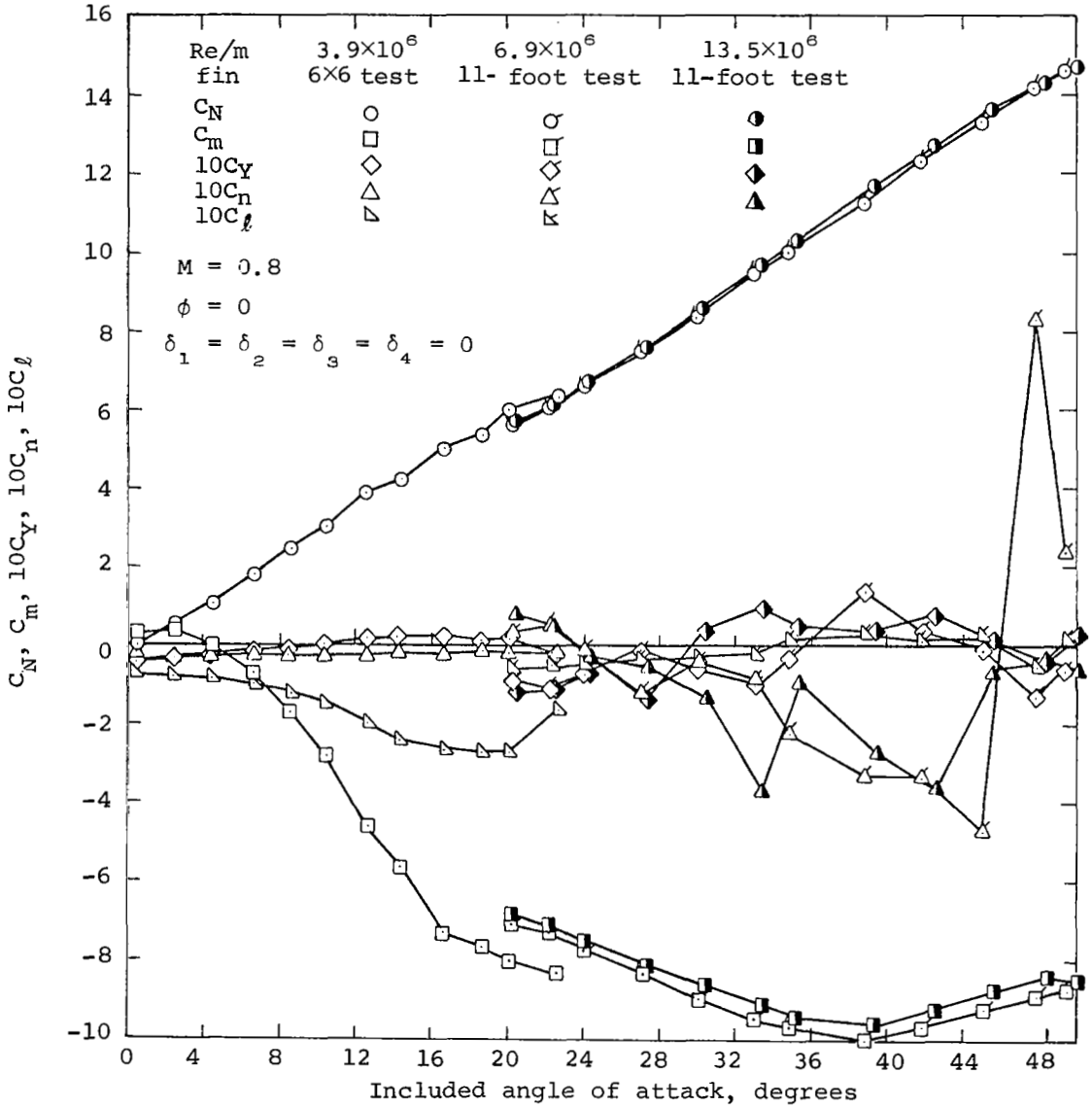

Figure 18.- Comparison of main balance data for 6- by 6- and 11-foot tests, body-canard-tail model.

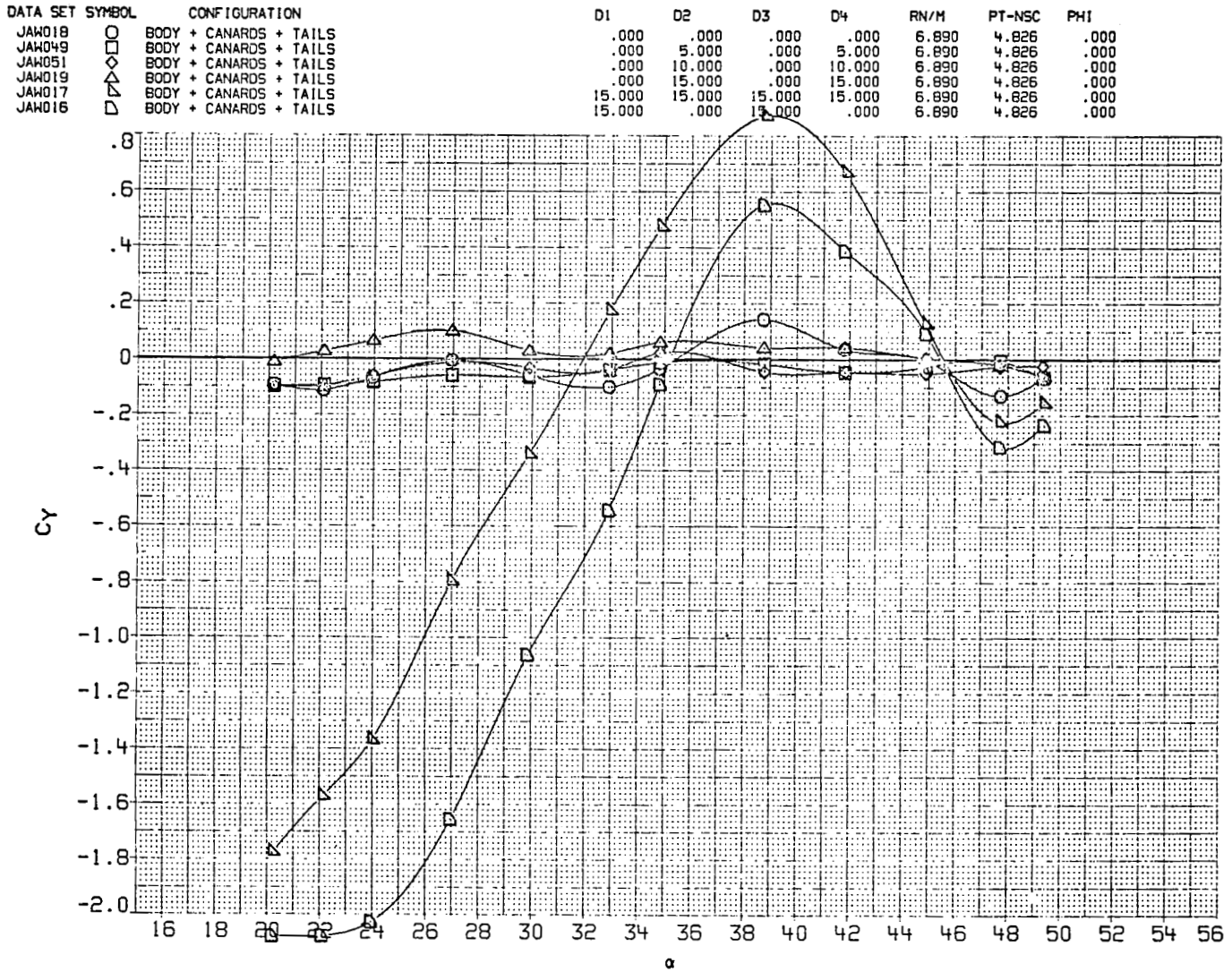

FIGURE 19 DATAMAN PLOT OF SIDE FORCE FOR BODY-CANARD-TAIL CONFIGURATION, M = 0.80

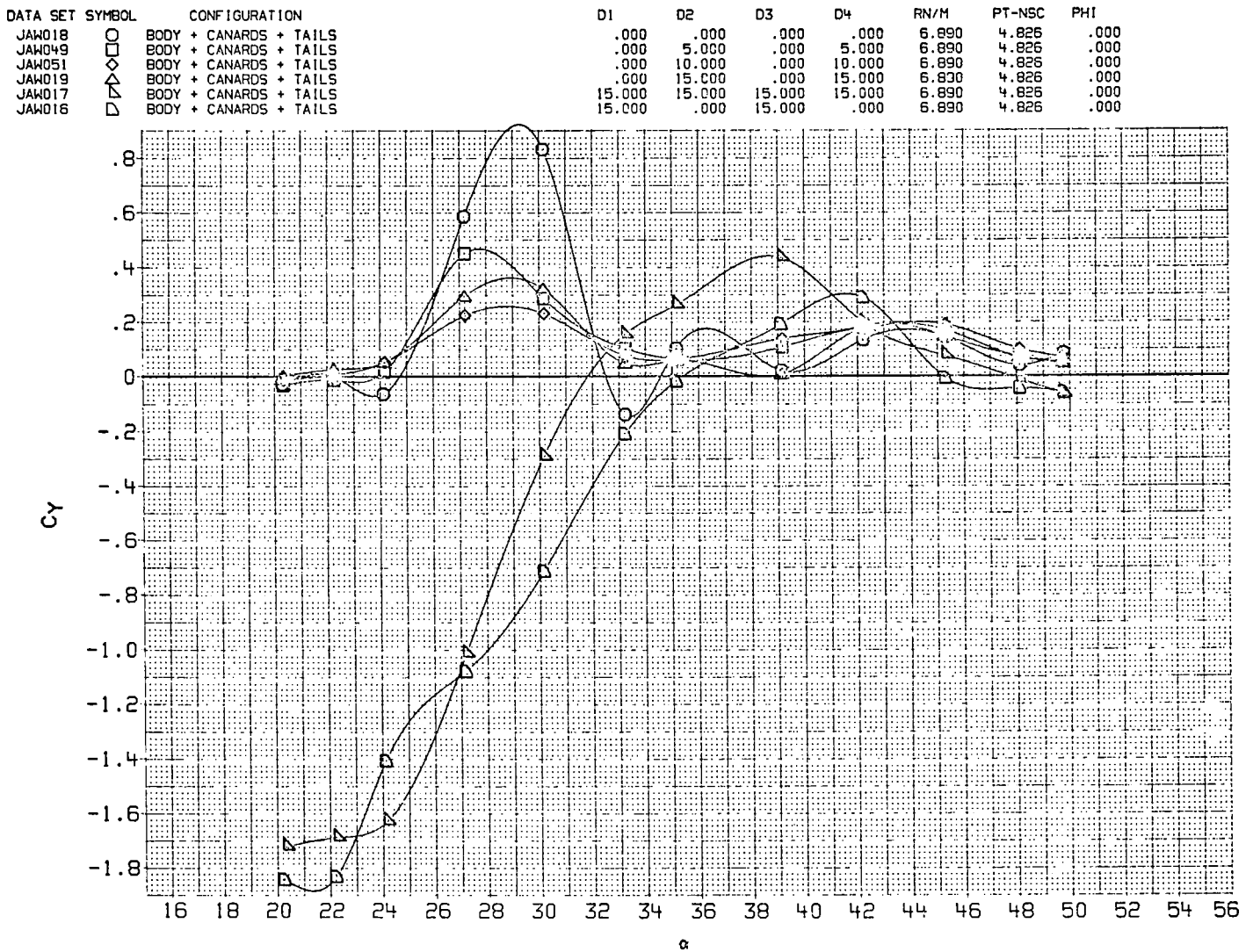

FIGURE 20 DATAMAN PLOT OF SIDE FORCE FOR BODY-CANARD-TAIL CONFIGURATION, M = 1.30

DATA SET	SYMBOL	CONFIGURATION	D1	D2	D3	D4	RN/M	PT-NSC	PHI
JAW018	○	BODY + CANARDS + TAILS	.000	.000	.000	.000	6.890	4.826	.000
JAW049	□	BODY + CANARDS + TAILS	.000	5.000	.000	5.000	6.890	4.826	.000
JAW051	◇	BODY + CANARDS + TAILS	.000	10.000	.000	10.000	6.890	4.826	.000
JAW019	△	BODY + CANARDS + TAILS	.000	15.000	.000	15.000	6.890	4.826	.000
JAW017	◁	BODY + CANARDS + TAILS	15.000	15.000	15.000	15.000	6.890	4.826	.000
JAW016	▷	BODY + CANARDS + TAILS	15.000	.000	15.000	.000	6.890	4.826	.000

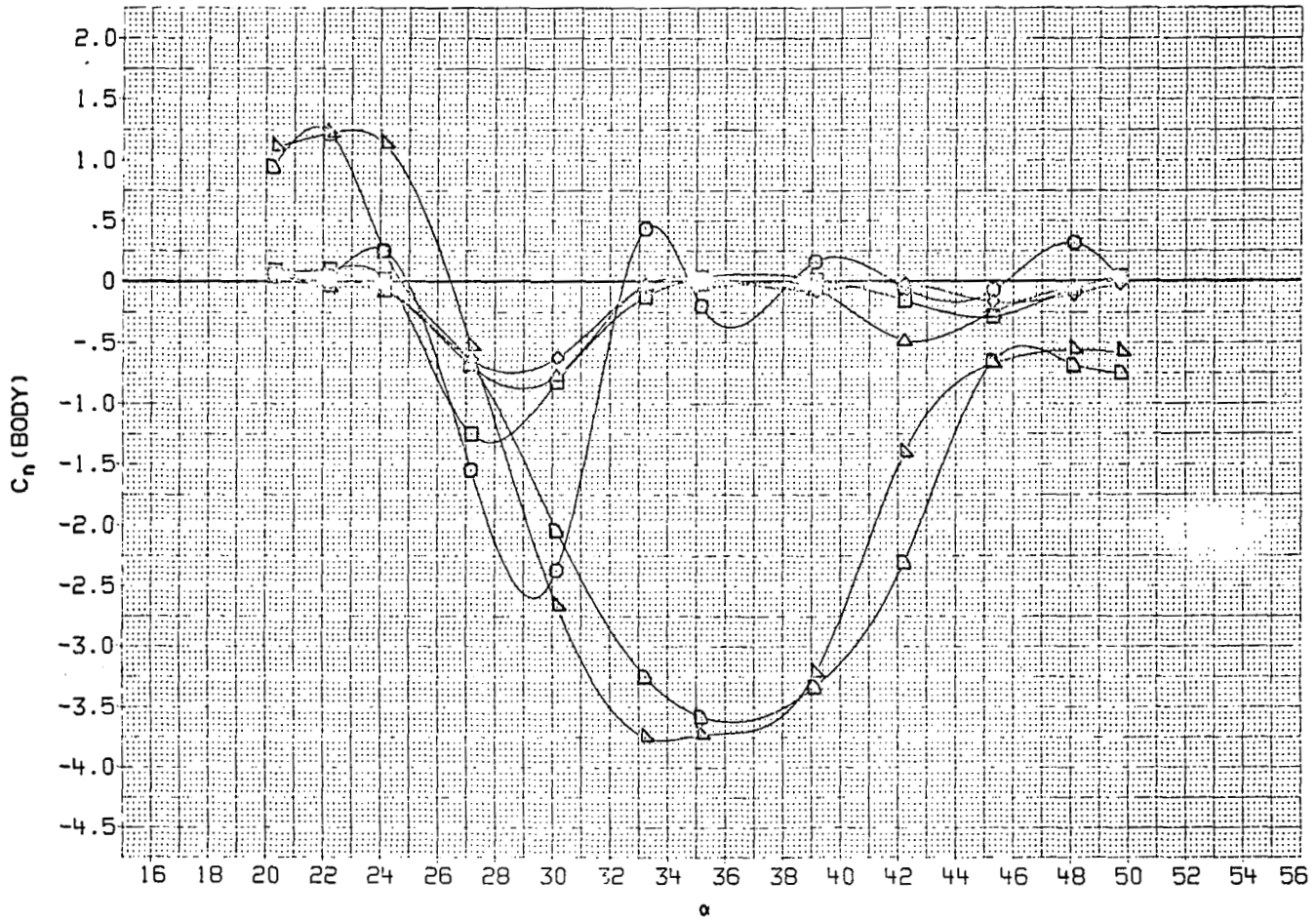

FIGURE 21 DATAMAN PLOT OF YAWING MOMENT FOR BODY-CANARD-TAIL CONFIGURATION, M = 1.30

DATA SET	SYMBOL	CONFIGURATION	D1	D2	D3	D4	RN/M	PT-NSC	PHI
JAW018	○	BODY + CANARDS + TAILS	.000	.000	.000	.000	6.890	4.826	.000
JAW049	□	BODY + CANARDS + TAILS	.000	5.000	.000	5.000	6.890	4.826	.000
JAW051	◇	BODY + CANARDS + TAILS	.000	10.000	.000	10.000	6.890	4.826	.000
JAW019	△	BODY + CANARDS + TAILS	.000	15.000	.000	15.000	6.890	4.826	.000
JAW017	◁	BODY + CANARDS + TAILS	15.000	15.000	15.000	15.000	6.890	4.826	.000
JAW016	D	BODY + CANARDS + TAILS	15.000	.000	15.000	.000	6.890	4.826	.000

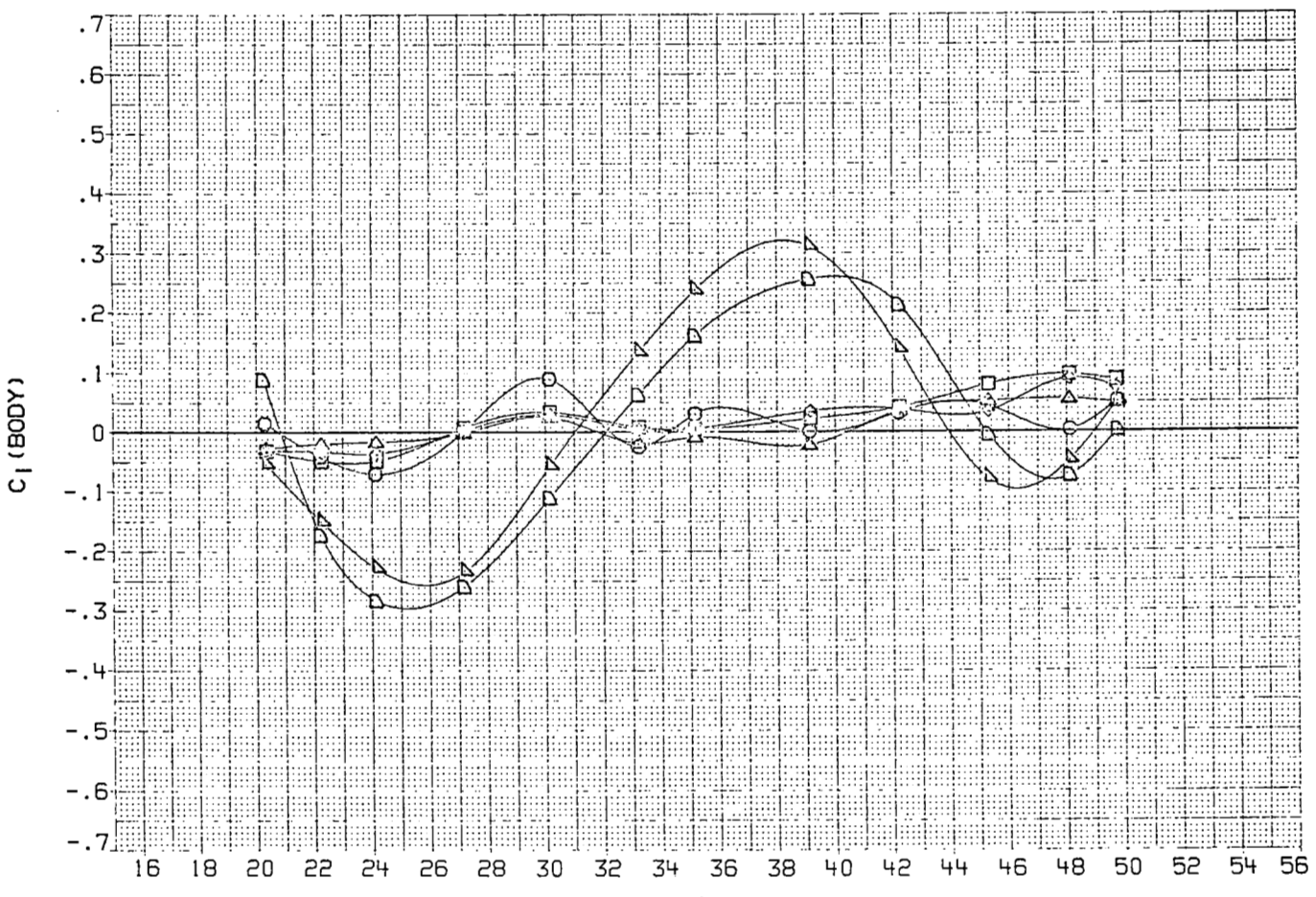

FIGURE 22 DATAMAN PLOT OF ROLLING MOMENT FOR BODY-CANARD-TAIL CONFIGURATION, M = 1.30

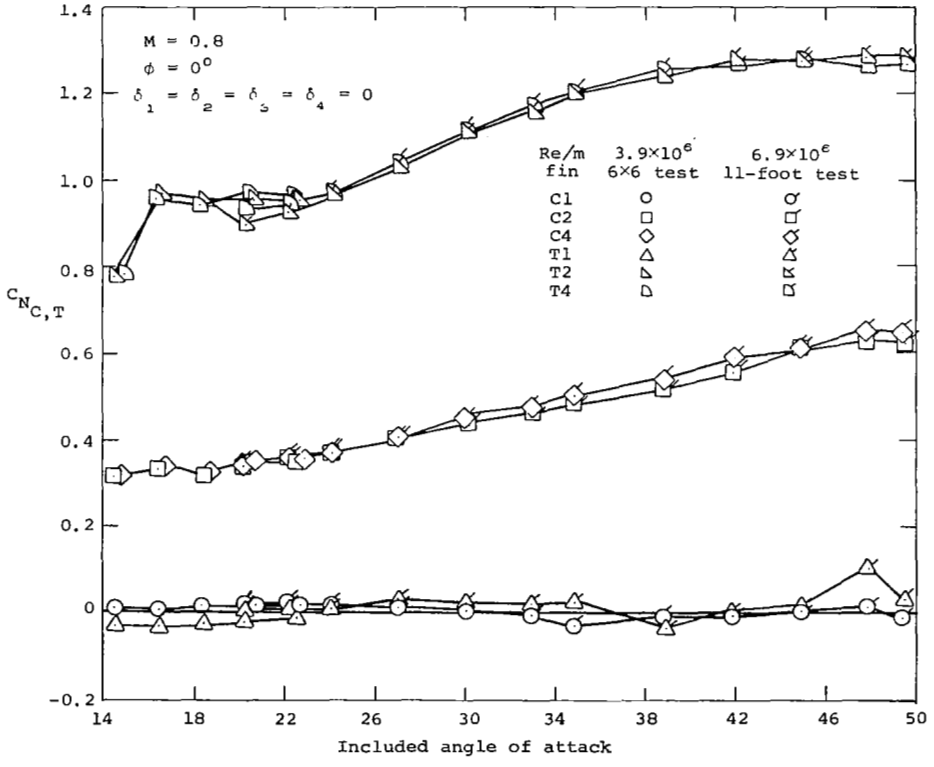

Figure 23.- Comparison of selected fin data for 6- by 6- and 11-foot tests, body-canard-tail model.

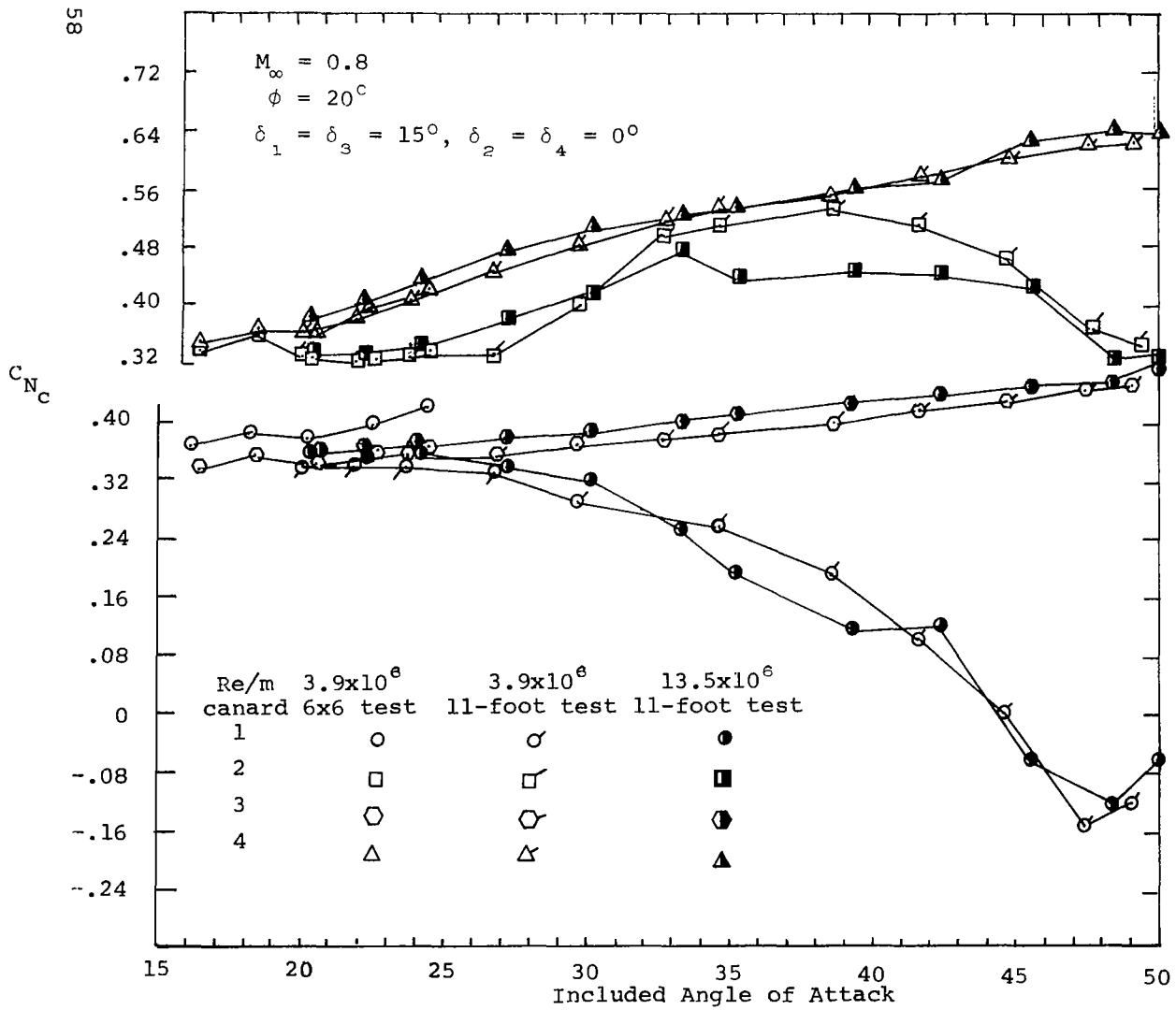

Figure 24 Comparison of canard balance data for 6- by 6 and 11-foot tests and Reynolds number effect, body-canard-tail model.

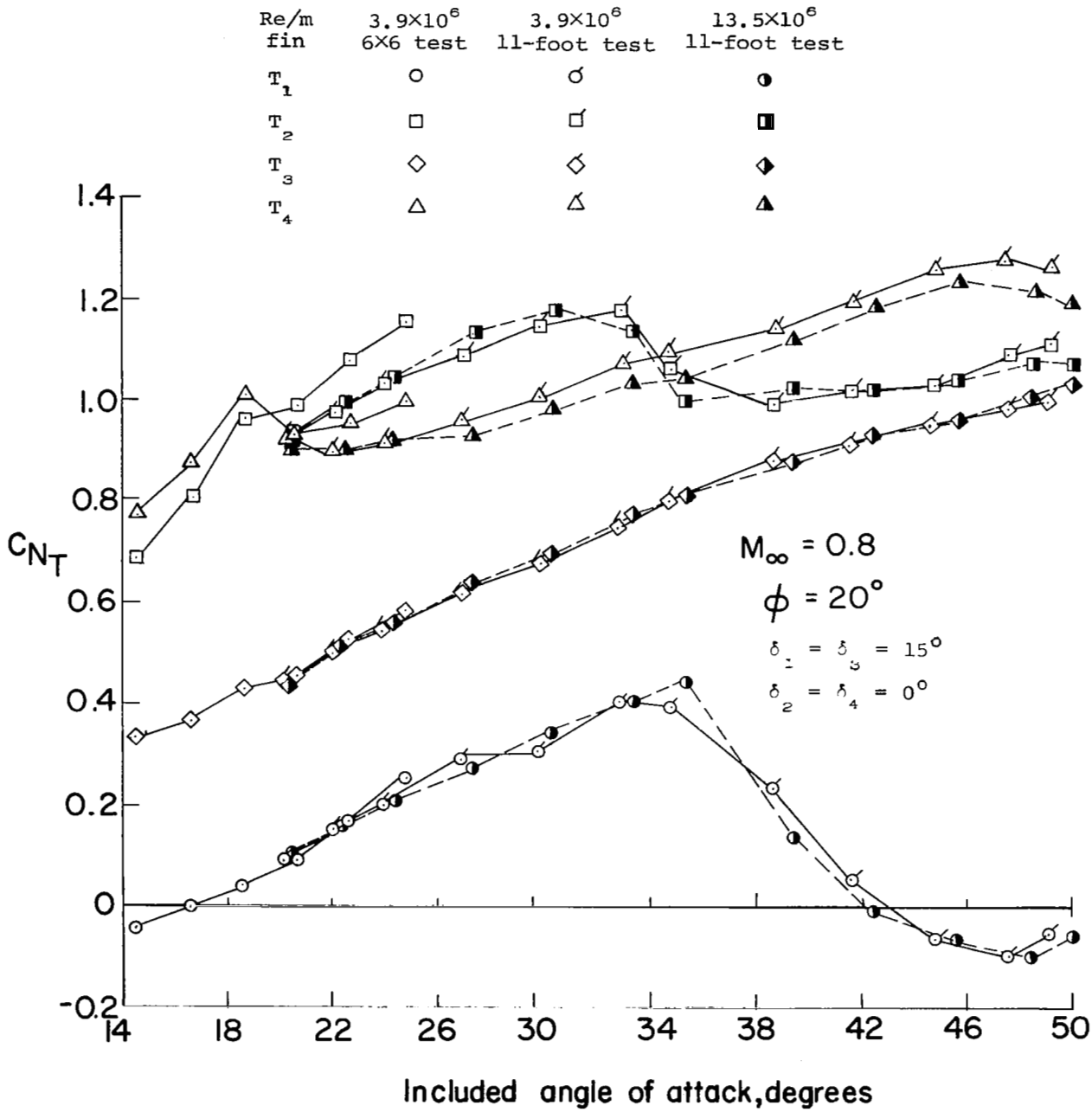

Figure 25.- Comparison of tail fin balance data for 6- by 6- and 11-foot tests for different Reynolds numbers. Body-canard-tail model.

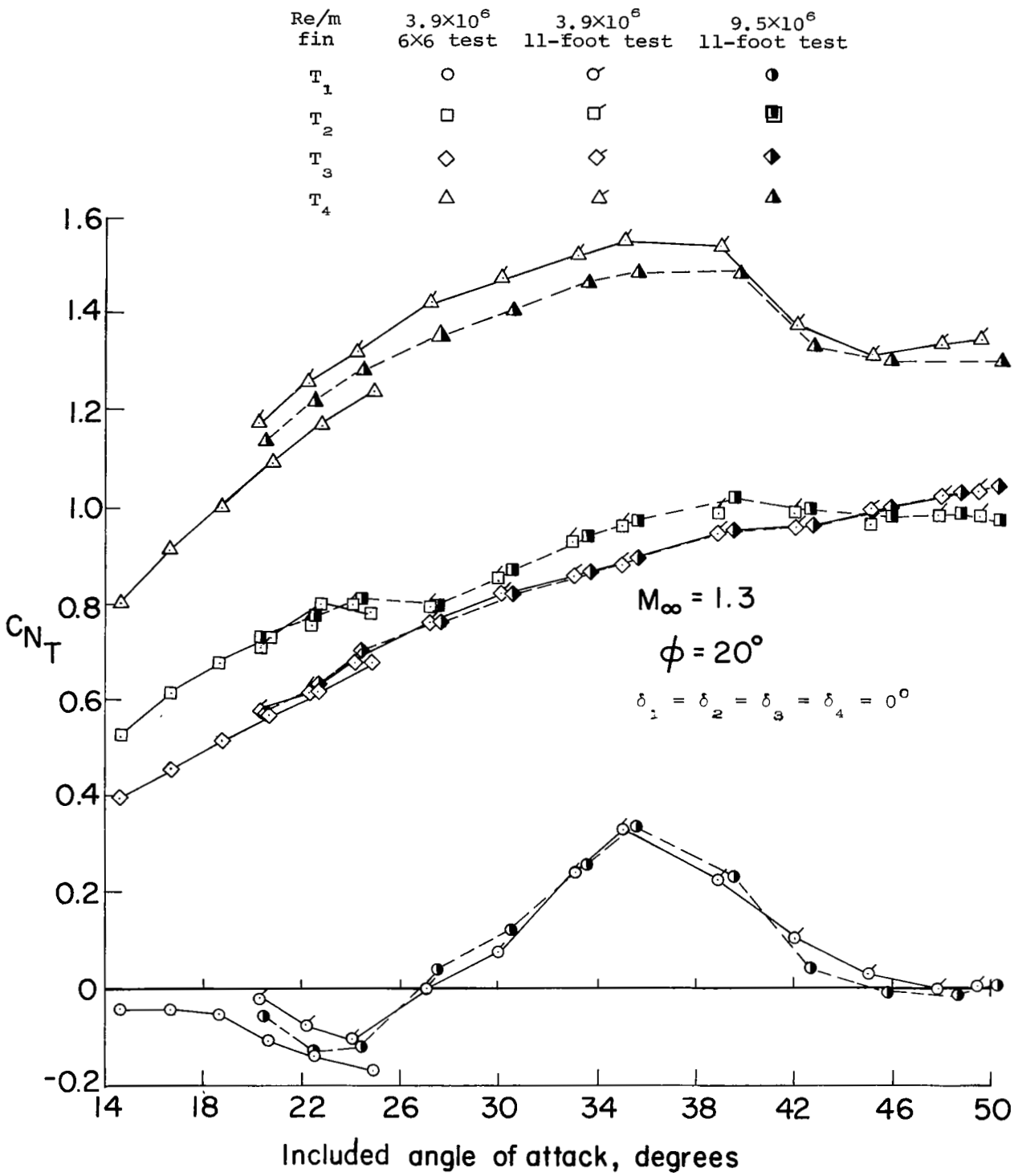

Figure 26.- Comparison of tail fin balance data for 6- by 6- and 11-foot tests for different Reynolds numbers. Body-canard-tail model.

DATA SET	SYMBOL	CONFIGURATION	D1	D2	D3	D4	RN/M	PT-NSC	PHI
JAW025	○	BODY + CANARDS + TAILS	.000	.000	.000	.000	6.890	4.826	20.000
JAW026	□	BODY + CANARDS + TAILS	.000	15.000	.000	15.000	6.890	4.826	20.000
JAW021	◇	BODY + CANARDS + TAILS	15.000	15.000	15.000	15.000	6.890	4.826	20.000
JAW022	△	BODY + CANARDS + TAILS	15.000	.000	15.000	.000	6.890	4.826	20.000

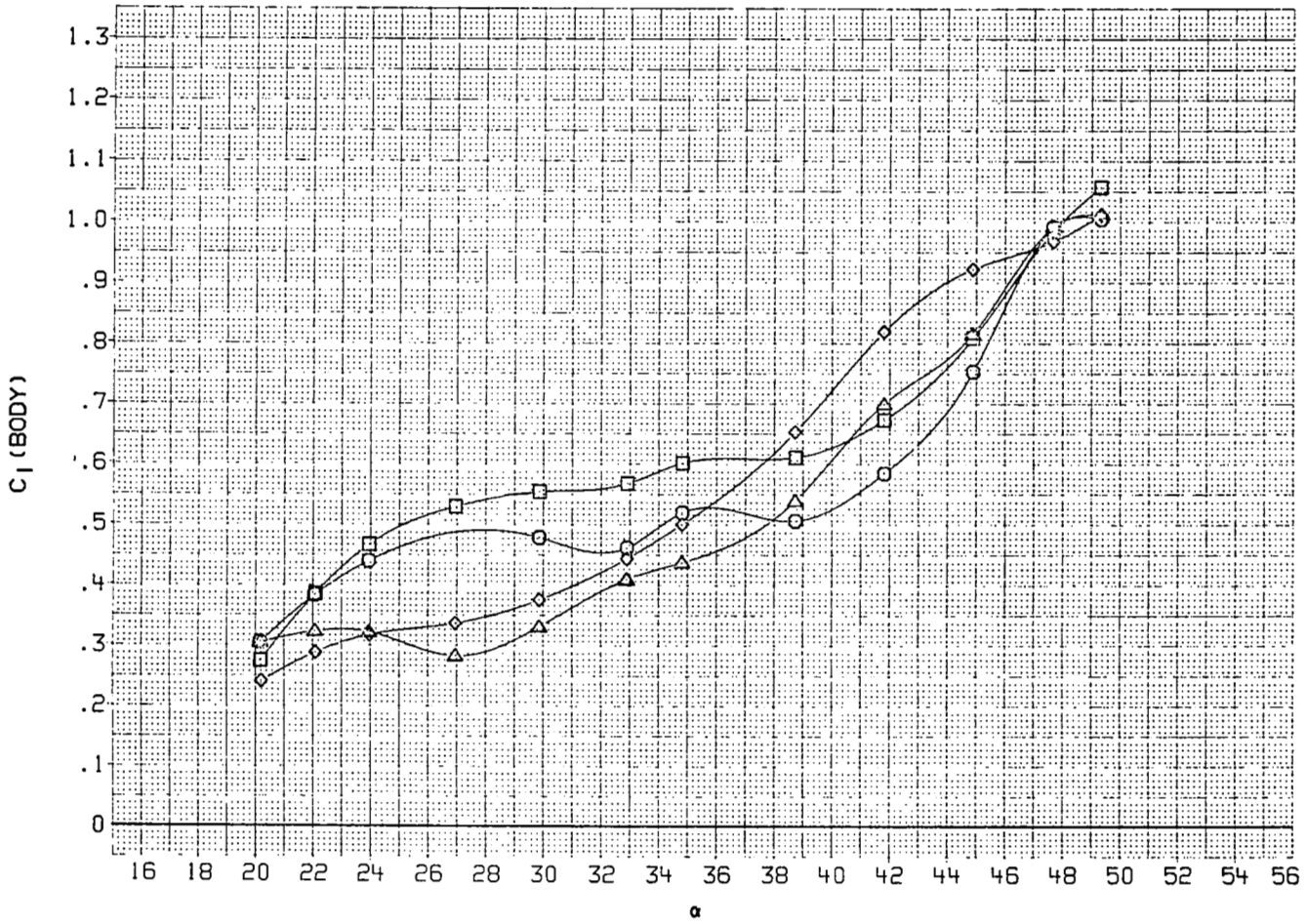

FIGURE 27 DATAMAN PLOT OF ROLLING MOMENT FOR BODY-CANARD-TAIL CONFIGURATION, M = 0,80

DATA SET	SYMBOL	CONFIGURATION	D1	D2	D3	D4	RN/M	PT-NSC	PHI
JAW039	○	BODY + CANARDS + TAILS	.000	.000	.000	.000	6.890	4.826	10.000
JAW040	□	BODY + CANARDS + TAILS	.000	15.000	.000	15.000	6.890	4.826	10.000
JAW038	◇	BODY + CANARDS + TAILS	15.000	15.000	15.000	15.000	6.890	4.826	10.000
JAW037	△	BODY + CANARDS + TAILS	15.000	.000	15.000	.000	6.890	4.826	10.000

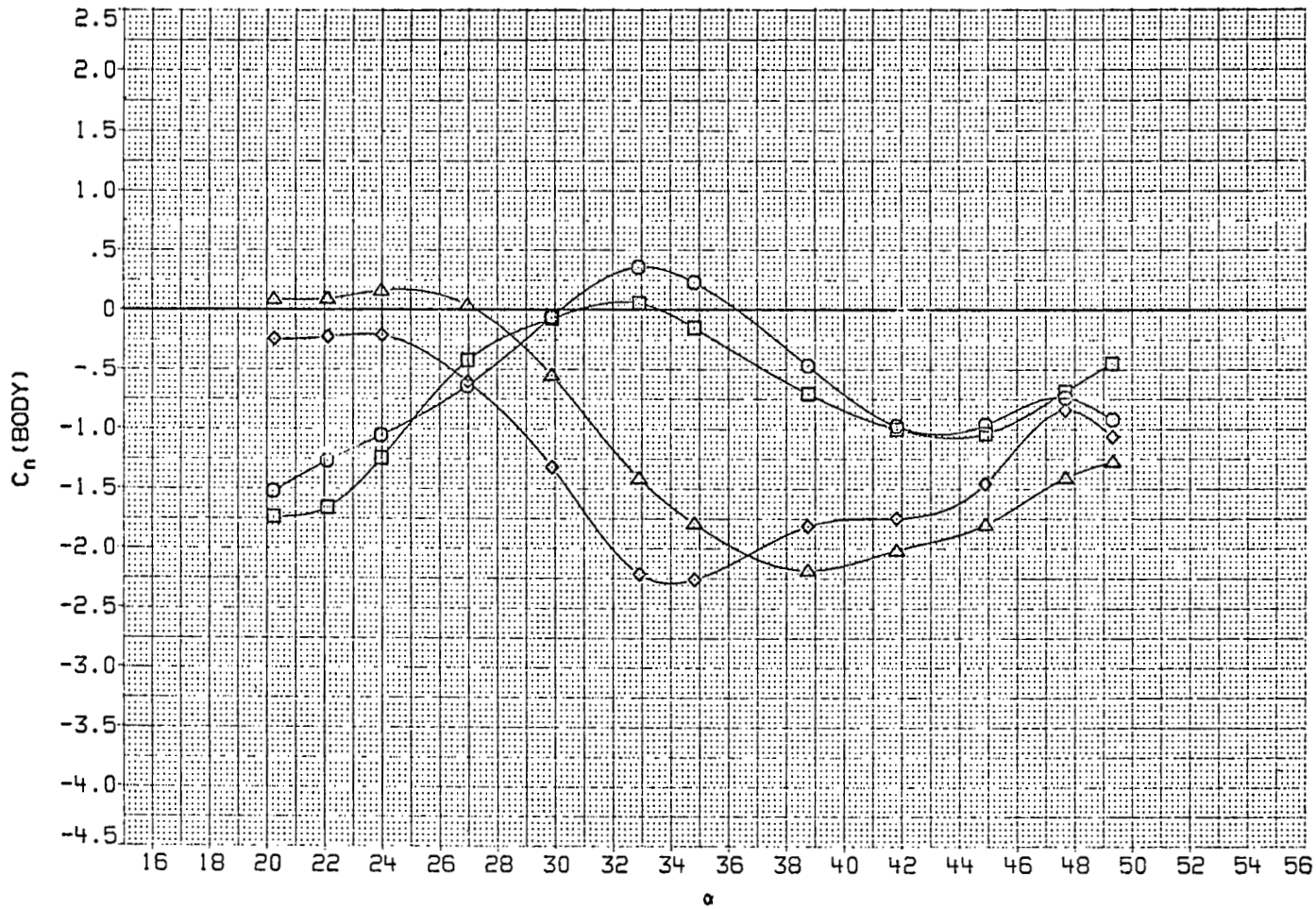

FIGURE 28 DATAMAN PLOT OF YAWING MOMENT FOR BODY-CANARD-TAIL CONFIGURATION, M = 0.80

DATA SET	SYMBOL	CONFIGURATION	D1	D2	D3	D4	RN/M	PT-NSC	PHI
JAW039	○	BODY + CANARDS + TAILS	.000	.000	.000	.000	6.890	4.826	10.000
JAW040	□	BODY + CANARDS + TAILS	.000	15.000	.000	15.000	6.890	4.826	10.000
JAW038	◇	BODY + CANARDS + TAILS	15.000	15.000	15.000	15.000	6.890	4.826	10.000
JAW037	△	BODY + CANARDS + TAILS	15.000	.000	15.000	.000	6.890	4.826	10.000

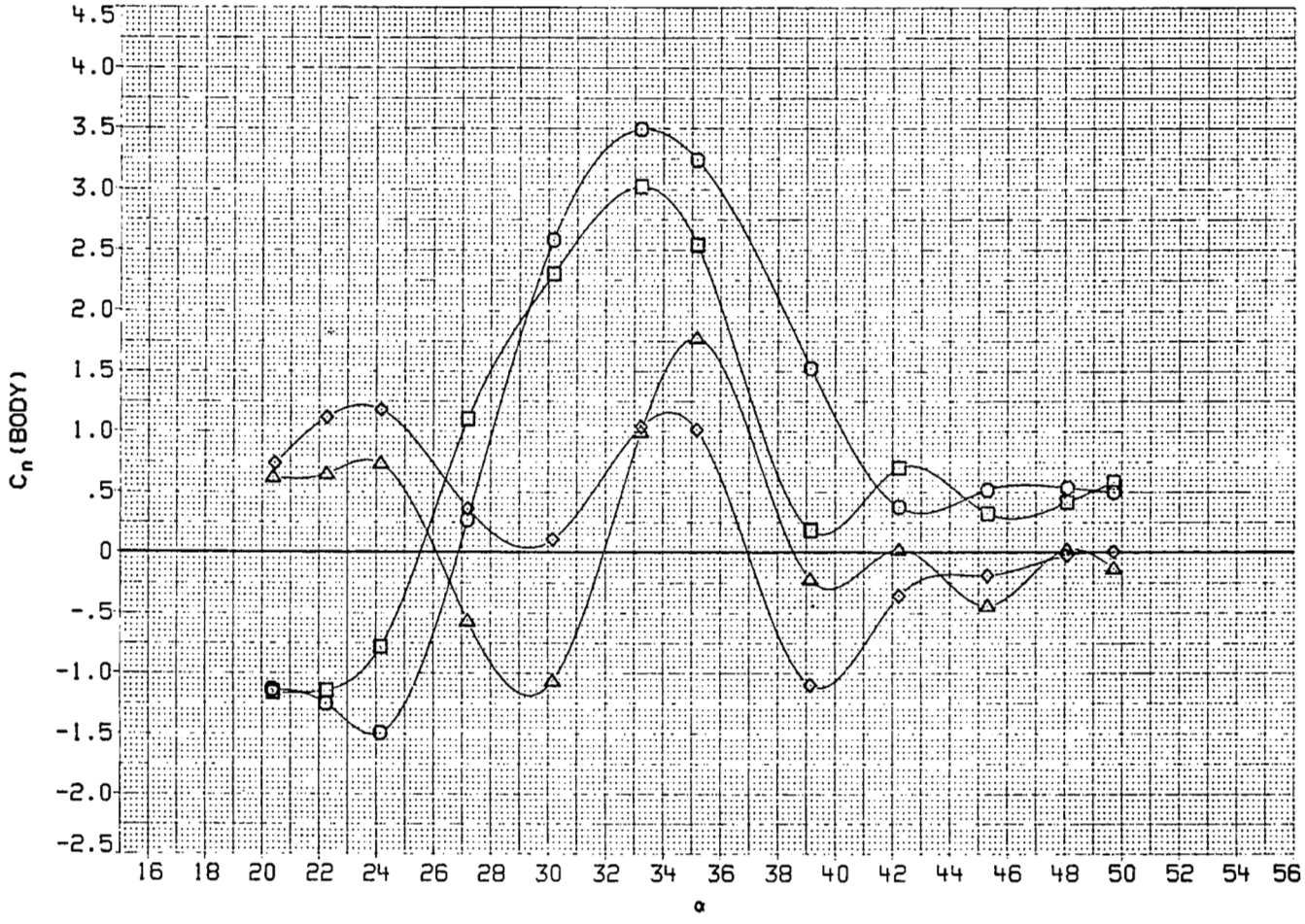

FIGURE 29 DATAMAN PLOT OF YAWING MOMENT FOR BODY-CANARD-TAIL CONFIGURATION, M = 1,30

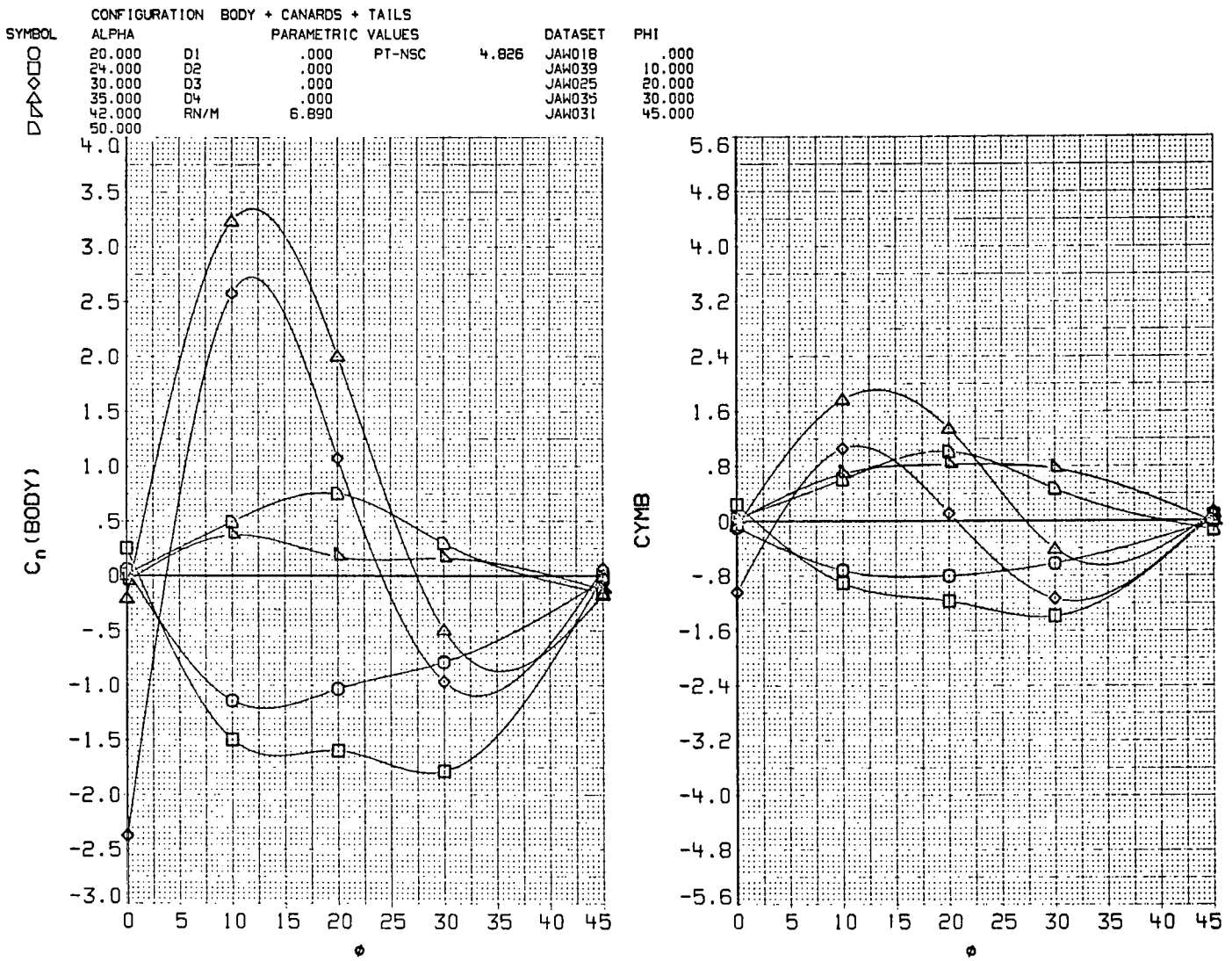

FIGURE 30 DATAMAN PLOTS SHOWING ROLL ANGLE EFFECTS FOR BODY-CANARD-TAIL CONFIGURATION, M = 1,3

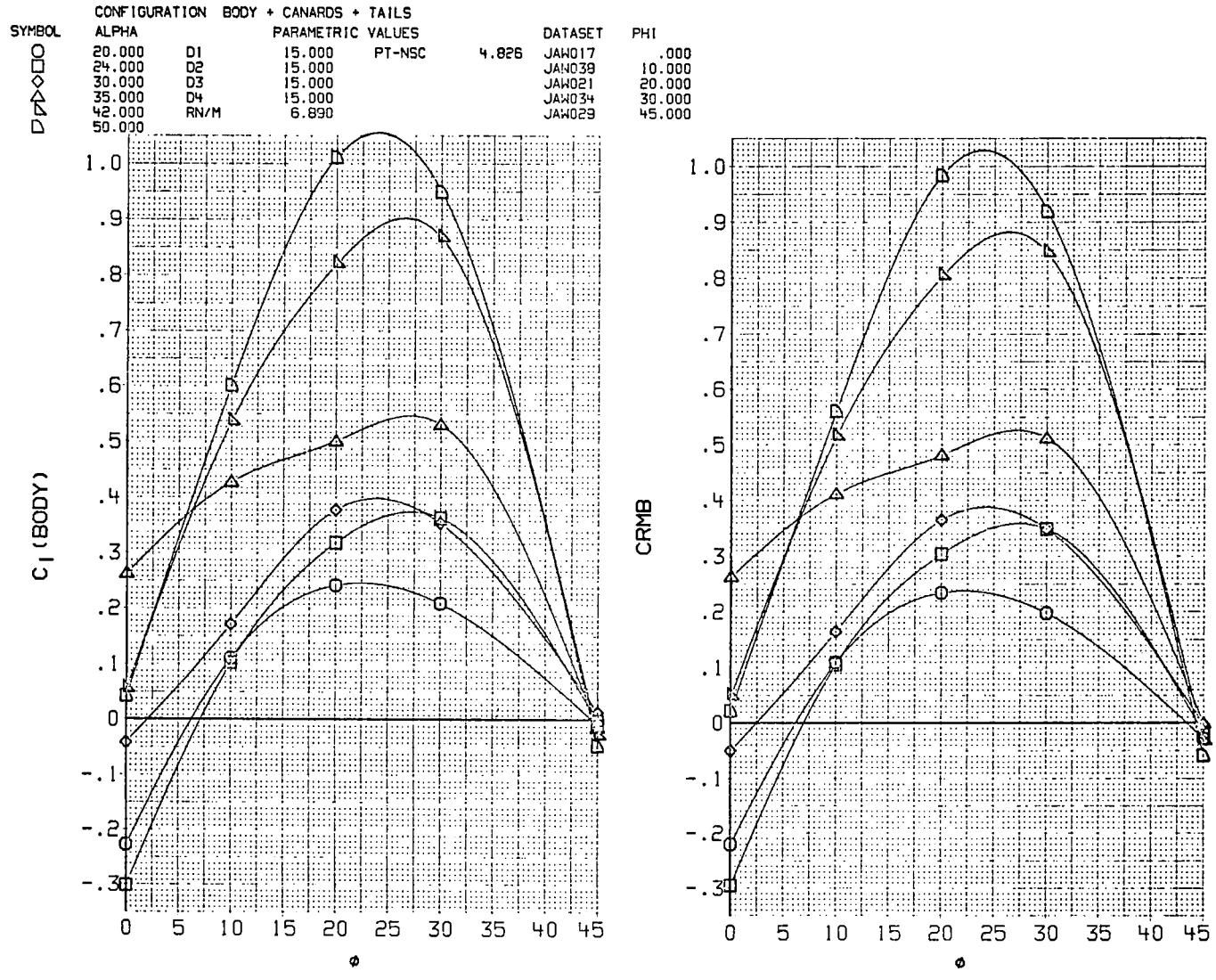

FIGURE 31 DATAMAN PLOTS SHOWING ROLL ANGLE EFFECTS FOR BODY-CANARD-TAIL CONFIGURATION, M = .80

DATA SET	SYMBOL	CONFIGURATION	RN/M	PT-NSC	PHI
JAW006	○	BODY + TAILS	3.937	2.758	20.000
JAW007	□	BODY + TAILS	6.890	4.826	20.000
JAW008	◇	BODY + TAILS	9.515	6.895	20.000

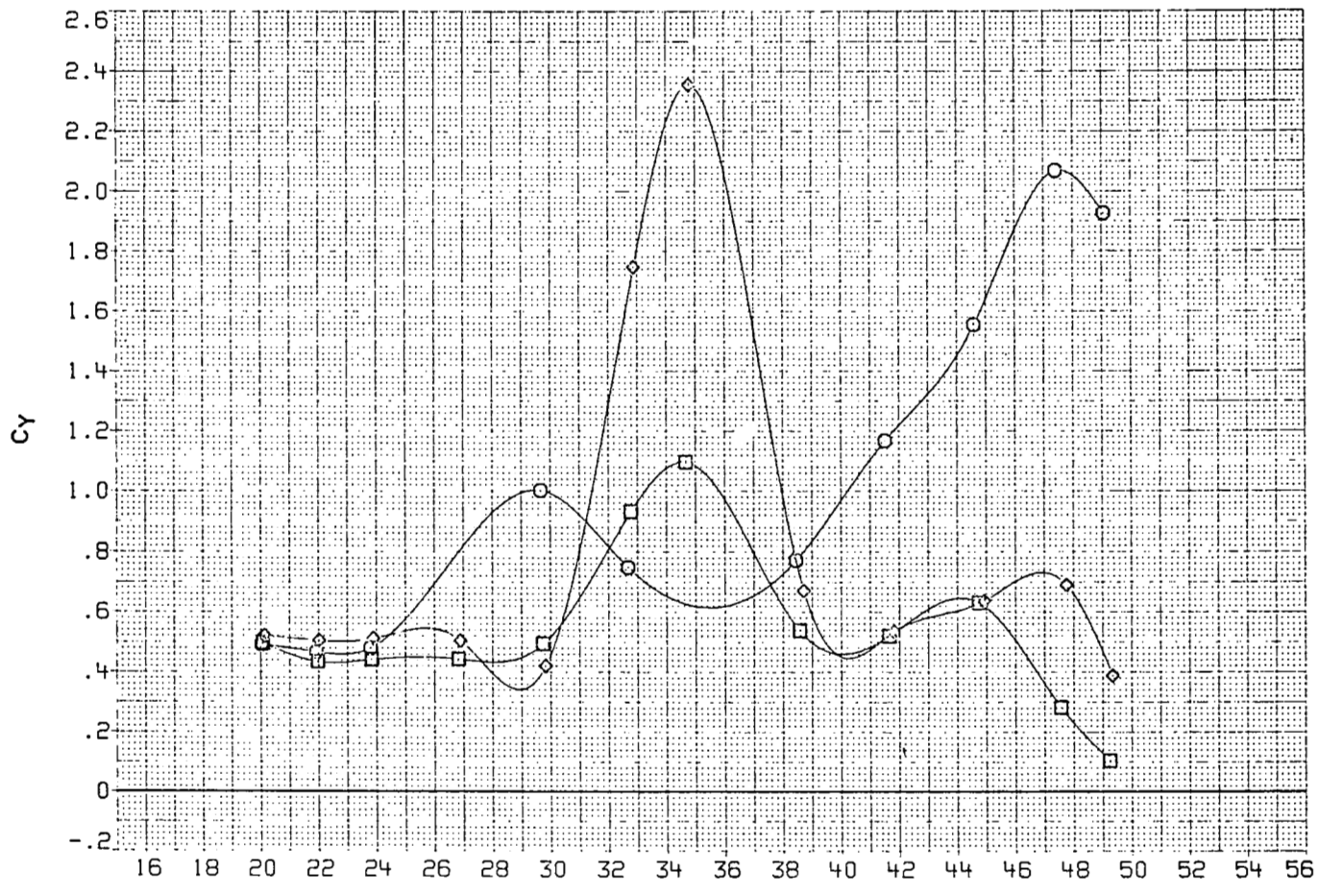

FIGURE 32 DATAMAN PLOT OF REYNOLDS NUMBER EFFECT FOR BODY-TAIL MODEL, M = 0,80, SIDE FORCE COEFFICIENT

DATA SET	SYMBOL	CONFIGURATION	RN/M	PT-NSC	PHI
JAW006	○	BODY + TAILS	3.937	2.758	20.000
JAW007	□	BODY + TAILS	6.890	4.826	20.000
JAW008	◇	BODY + TAILS	9.515	6.895	20.000

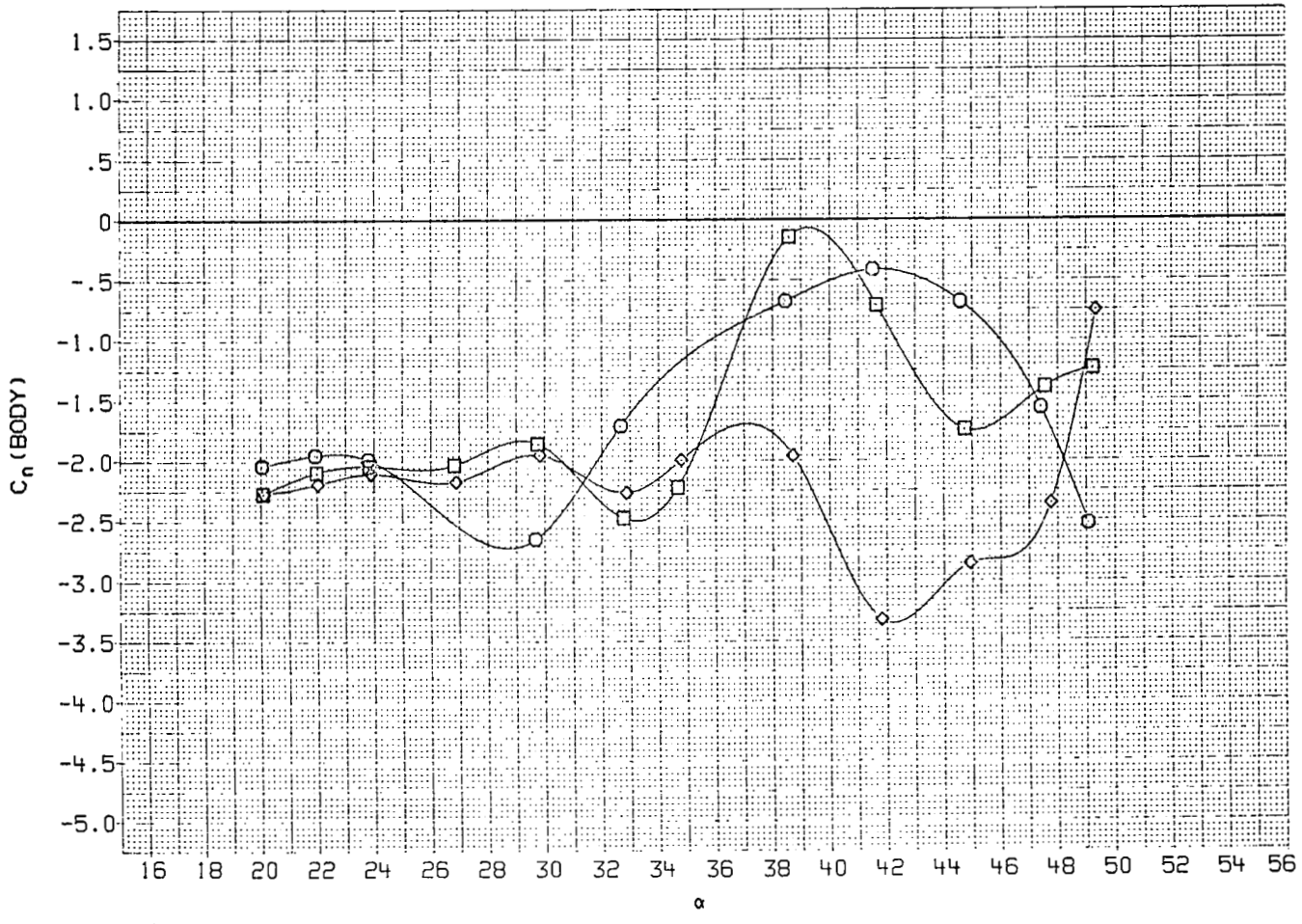

FIGURE 33 DATAMAN PLOT OF REYNOLDS NUMBER EFFECT FOR BODY-TAIL MODEL, M = 0,80, YAWING MOMENT COEFFICIENT

DATA SET	SYMBOL	CONFIGURATION	D1	D2	D3	D4	RN/M	PT-NSC	PHI
JAW044	○	BODY + CANARDS + TAILS	15.000	.000	15.000	.000	3.937	2.758	20.000
JAW022	□	BODY + CANARDS + TAILS	15.000	.000	15.000	.000	6.890	4.826	20.000
JAW043	◇	BODY + CANARDS + TAILS	15.000	.000	15.000	.000	9.515	6.895	20.000
JAW045	△	BODY + CANARDS + TAILS	15.000	.000	15.000	.000	13.452	10.342	20.000

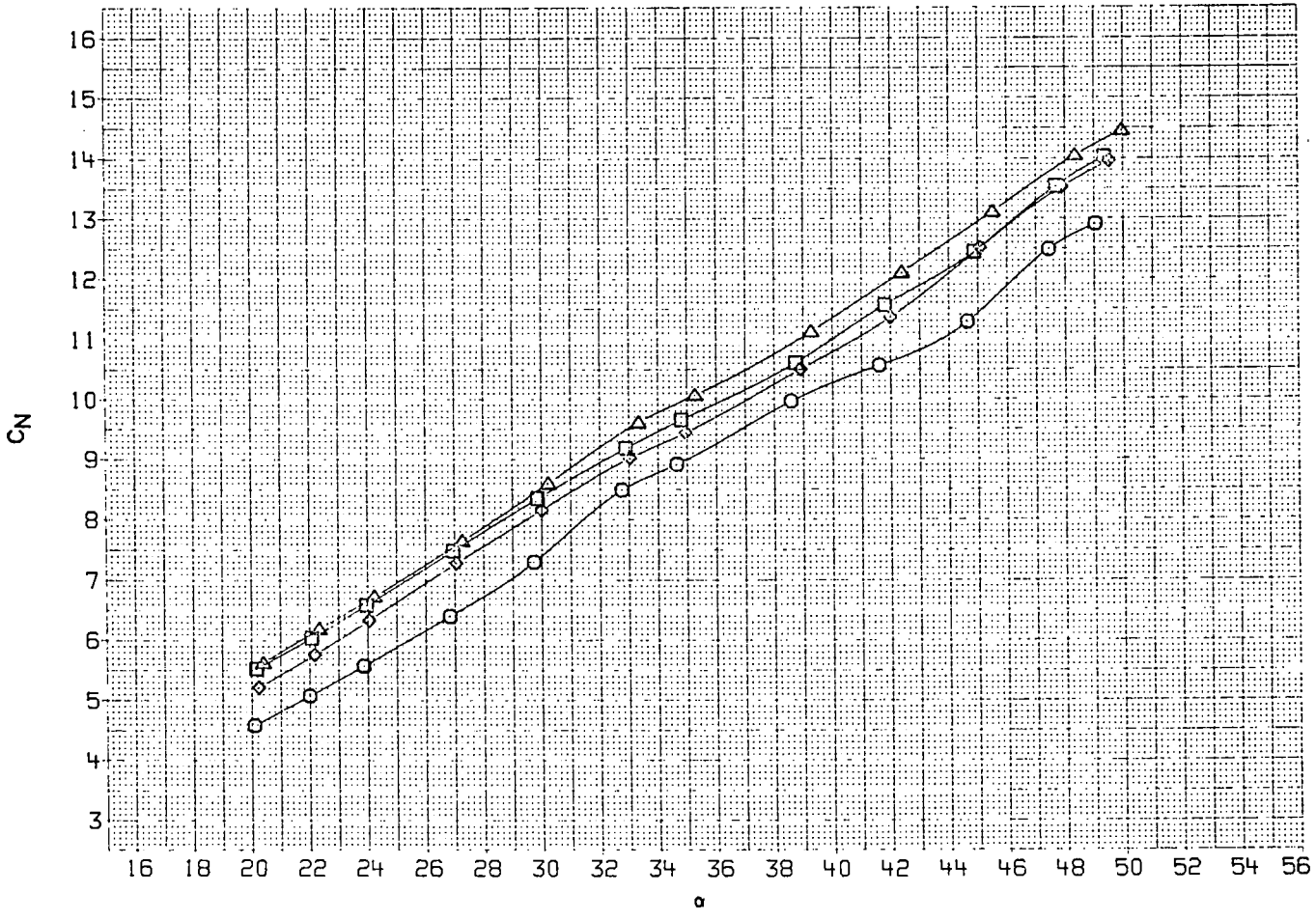

FIGURE 34 DATAMAN PLOT OF REYNOLDS NUMBER EFFECT ON BODY-CANARD-TAIL MODEL, M = 0,80, NORMAL FORCE COEFFICIENT

DATA SET	SYMBOL	CONFIGURATION	D1	D2	D3	D4	RN/M	PT-NSC	PHI
JAW044	○	BODY + CANARDS + TAILS	15.000	.000	15.000	.000	3.937	2.758	20.000
JAW022	□	BODY + CANARDS + TAILS	15.000	.000	15.000	.000	6.890	4.826	20.000
JAW043	◇	BODY + CANARDS + TAILS	15.000	.000	15.000	.000	9.515	6.895	20.000
JAW045	△	BODY + CANARDS + TAILS	15.000	.000	15.000	.000	13.452	10.342	20.000

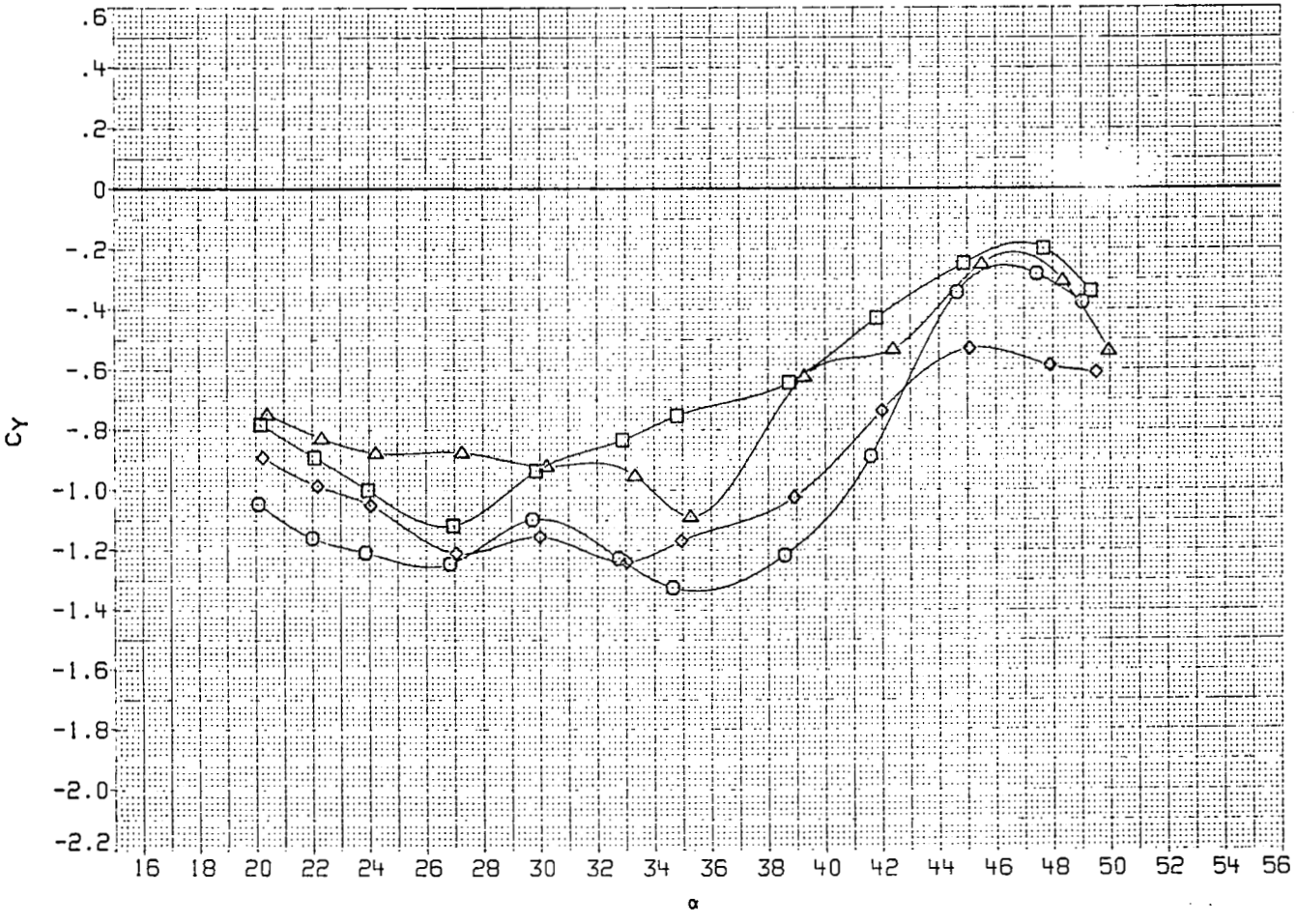

FIGURE 35 DATAMAN PLOT OF REYNOLDS NUMBER EFFECT FOR BODY-CANARD-TAIL MODEL, M = 0.80, SIDE FORCE COEFFICIENT

DATA SET	SYMBOL	CONFIGURATION	Specific Humidity	D1	D2	D3	D4	RN/M	PT-NSC	PHI
KAW018	○	BODY + CANARDS + TAILS	0	.000	.000	.000	.000	6.890	4.826	.000
KAW056	□	BODY + CANARDS + TAILS	.00058	.000	.000	.000	.000	6.890	4.826	.000
KAW016	◇	BODY + CANARDS + TAILS	0	15.000	.000	15.000	.000	6.890	4.826	.000
KAW055	△	BODY + CANARDS + TAILS	.00063	15.000	.000	15.000	.000	6.890	4.826	.000

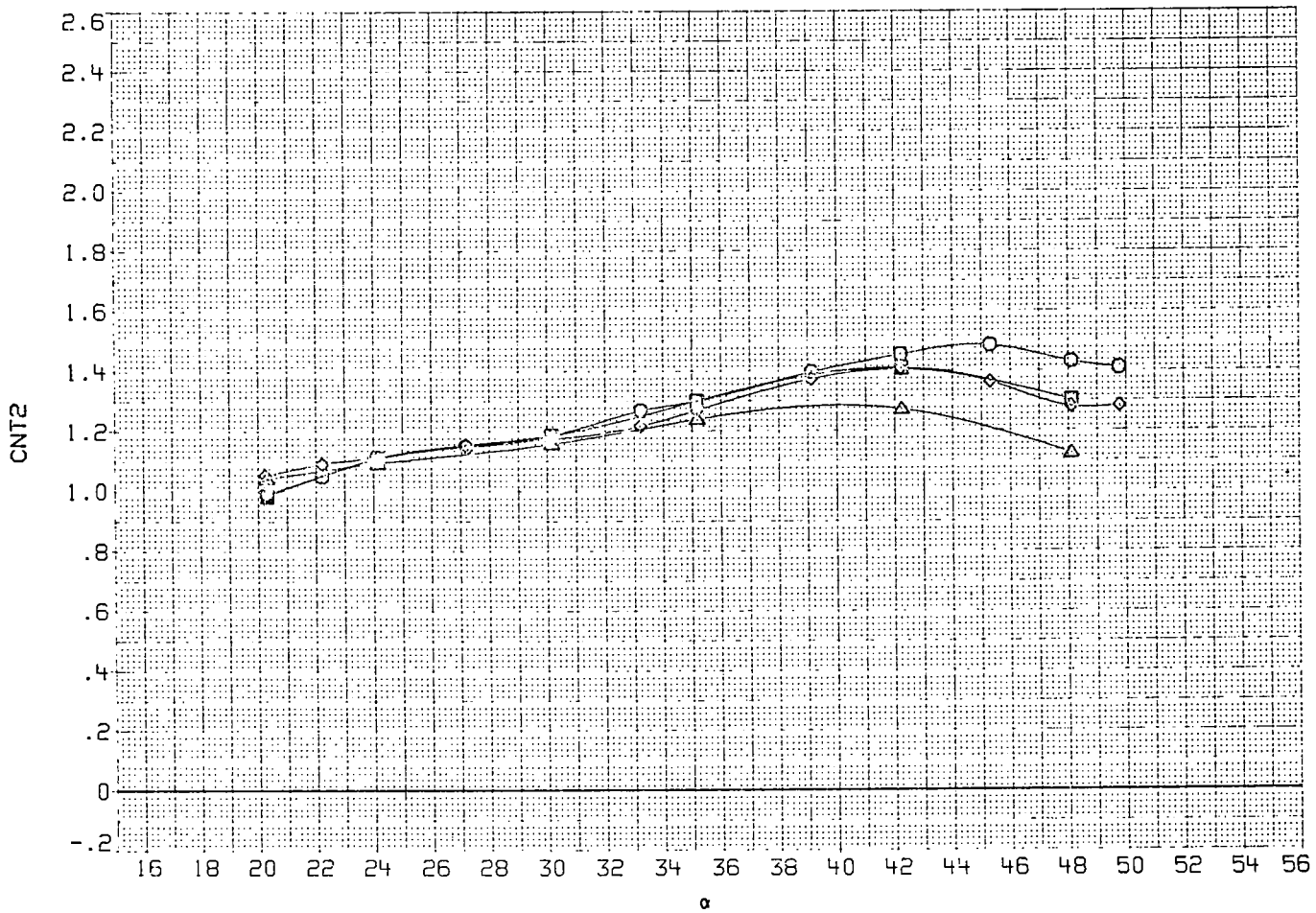

FIGURE 36 DATAMAN PLOT OF THE EFFECT OF VAPOR SCREEN CONDITIONS ON TAIL 2 NORMAL FORCE, M = 1.30

DATA SET	SYMBOL	CONFIGURATION	Specific Humidity	D1	D2	D3	D4	RN/M	PT-NSC	PHI
JAW025	○	BODY + CANARDS + TAILS	0	.000	.000	.000	.000	6.890	4.826	20.000
JAW058	□	BODY + CANARDS + TAILS	.00039	.000	.000	.000	.000	6.890	4.826	20.000
JAW042	◇	BODY + CANARDS + TAILS	0	15.000	.000	15.000	.000	6.890	4.826	20.000
JAW059	△	BODY + CANARDS + TAILS	.00039	15.000	.000	15.000	.000	6.890	4.826	20.000

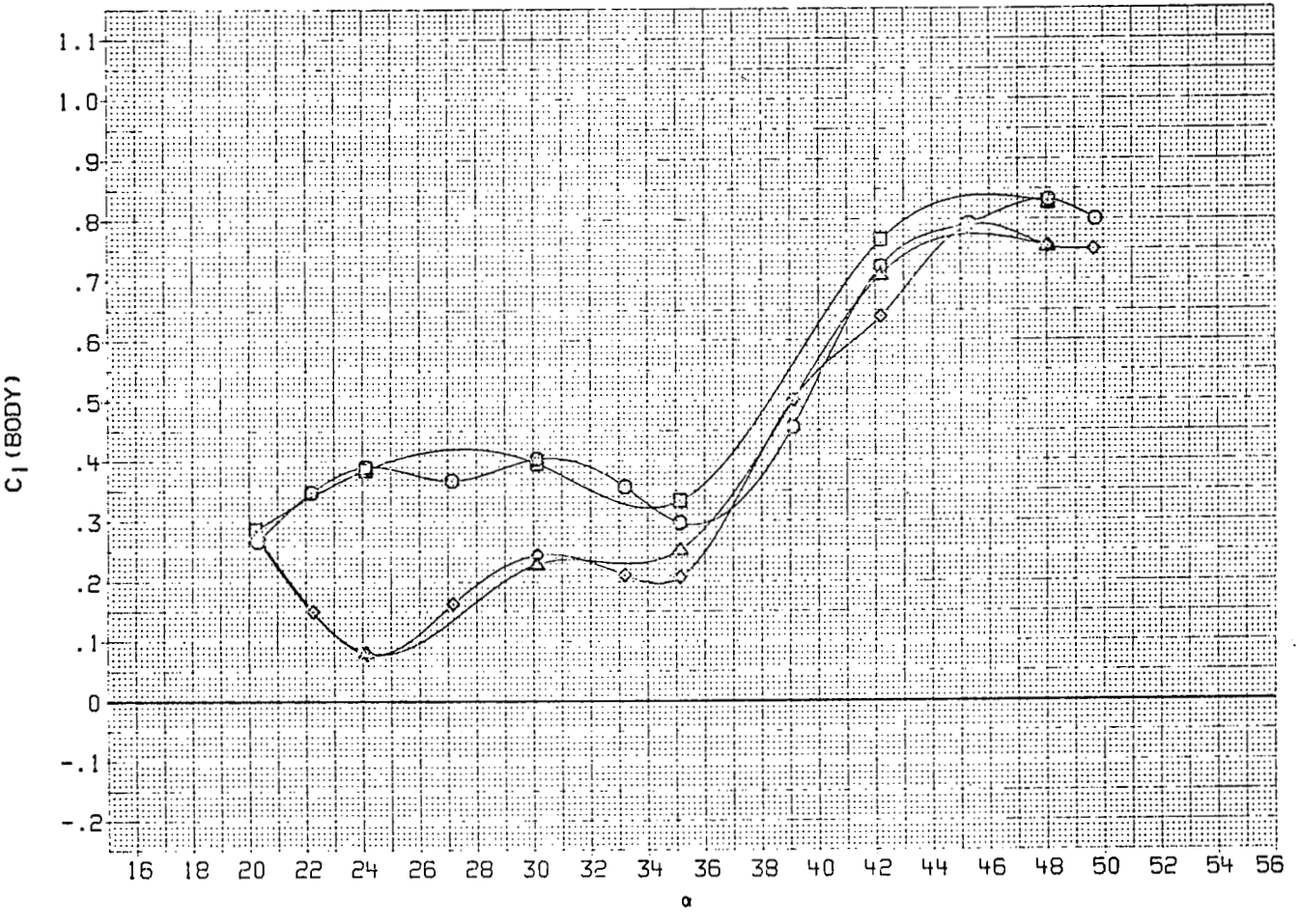

FIGURE 37 DATAMAN PLOT OF VAPOR SCREEN CONDITIONS ON ROLL, M = 1.30

DATA SET	SYMBOL	CONFIGURATION	Specific Humidity	D1	D2	D3	D4	RN/M	PT-NSC	PHI
JAW025	○	BODY + CANARDS + TAILS	0	.000	.000	.000	.000	6.890	4.826	20.000
JAW038	□	BODY + CANARDS + TAILS	.00039	.000	.000	.000	.000	6.890	4.826	20.000
JAW042	◇	BODY + CANARDS + TAILS	0	15.000	.000	15.000	.000	6.890	4.826	20.000
JAW039	△	BODY + CANARDS + TAILS	.00039	15.000	.000	15.000	.000	6.890	4.826	20.000

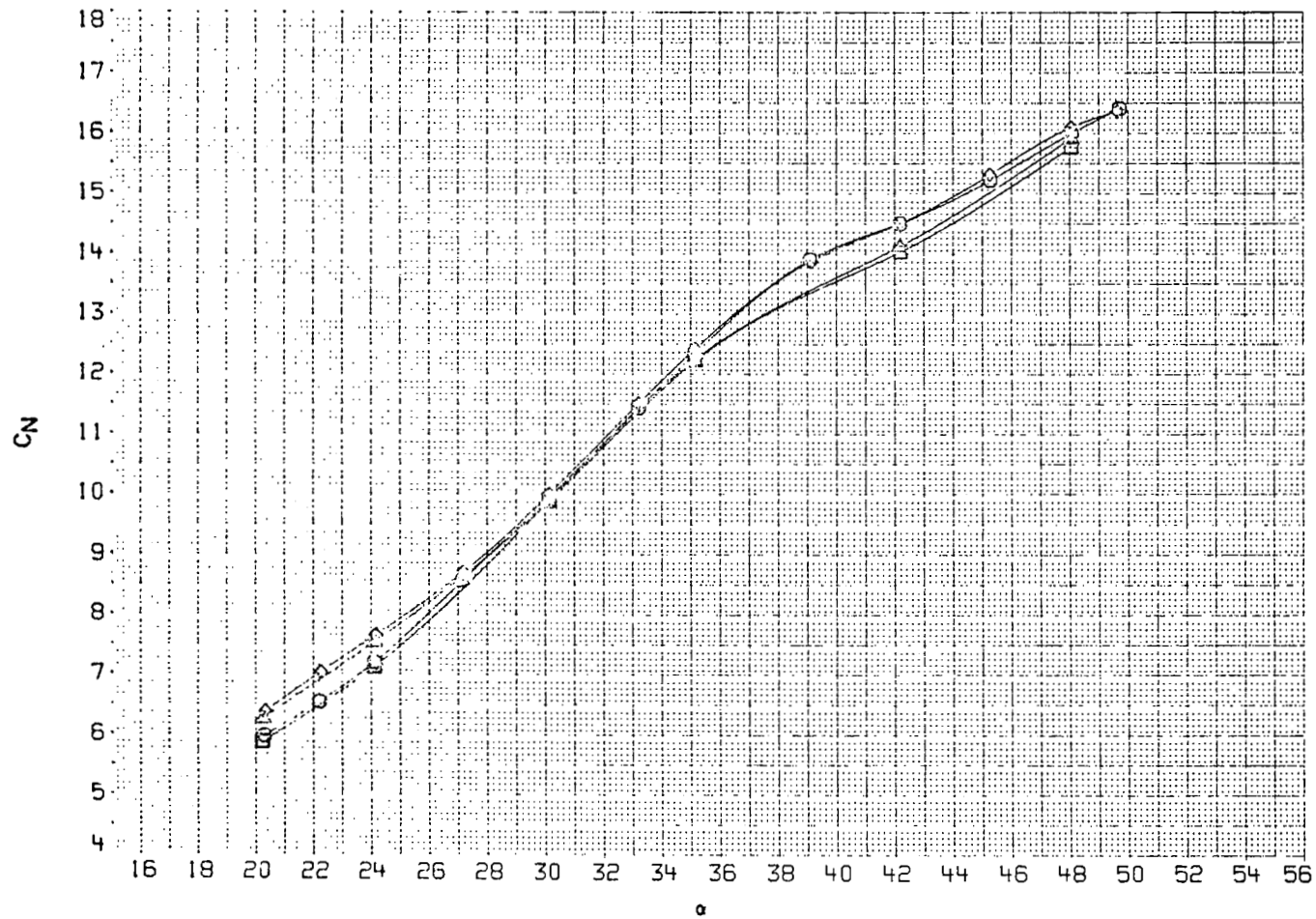

FIGURE 38 DATAMAN PLOT OF EFFECT OF VAPOR SCREEN CONDITIONS ON NORMAL FORCE, M = 1.30

DATA SET	SYMBOL	CONFIGURATION	Specific Humidity	D1	D2	D3	D4	RN/M	PT-NSC	PHI
JAW025	○	BODY + CANARDS + TAILS	0	.000	.000	.000	.000	6.890	4.826	20.000
JAW059	□	BODY + CANARDS + TAILS	.00039	.000	.000	.000	.000	6.890	4.826	20.000
JAW042	◇	BODY + CANARDS + TAILS	0	15.000	.000	15.000	.000	6.890	4.826	20.000
JAW059	△	BODY + CANARDS + TAILS	.00039	15.000	.000	15.000	.000	6.890	4.826	20.000

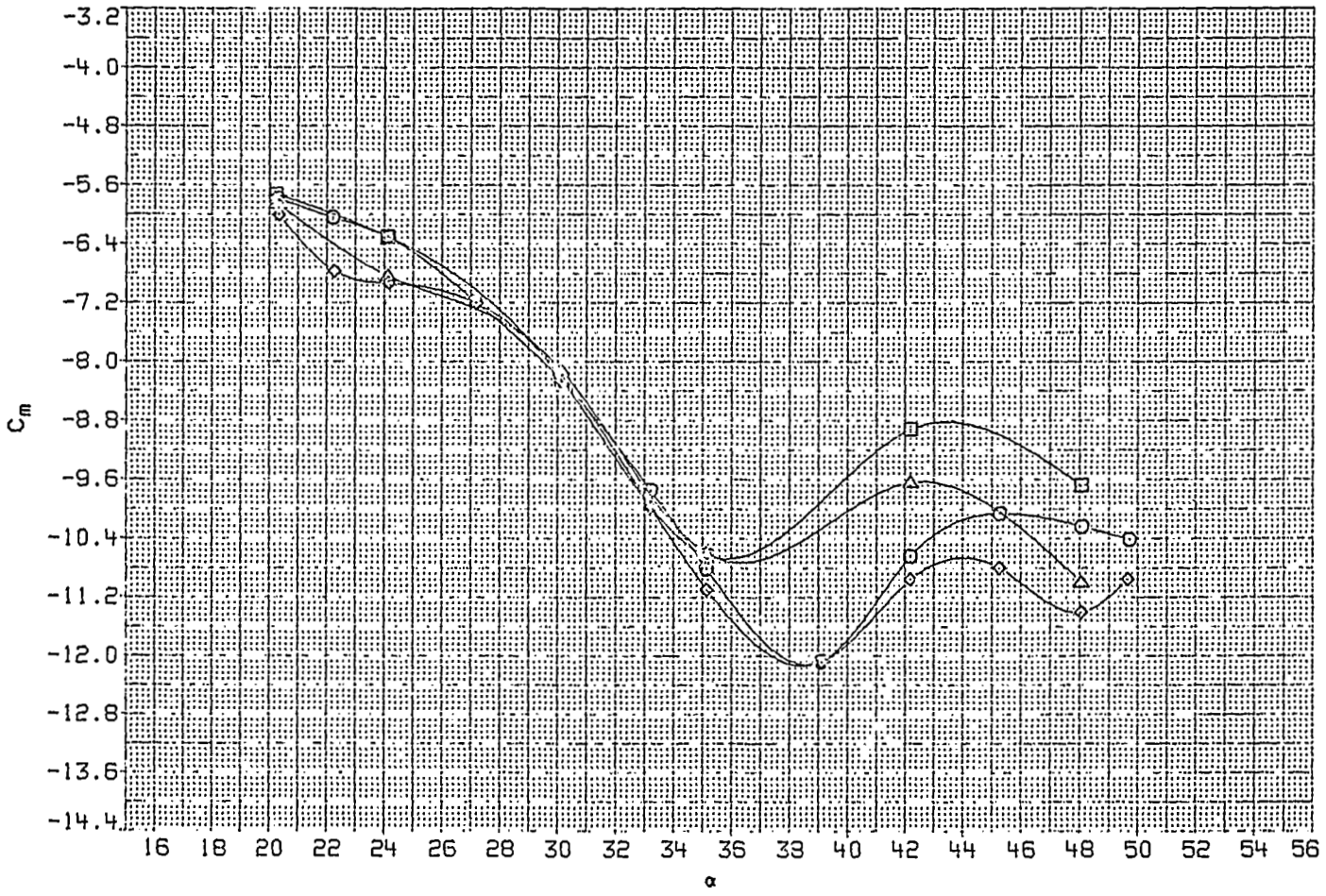

FIGURE 39 DATAMAN PLOT OF THE EFFECT OF VAPOR SCREEN CONDITIONS ON PITCHING MOMENT, M = 1.30

1. Report No.	2. Government Accession No.	3. Recipient's Catalog No.
CR-2993		

4. Title and Subtitle	5. Report Date
HIGH ANGLE CANARD MISSILE TEST IN THE AMES 11-FOOT TRANSONIC WIND TUNNEL	June 1978
	6. Performing Organization Code
7. Author(s)	8. Performing Organization Report No.
Richard G. Schwind	NEAR TR 134
	10. Work Unit No.
9. Performing Organization Name and Address Nielsen Engineering & Research, Inc. 510 Clyde Avenue Mountain View, CA 94043	11. Contract or Grant No. NAS2-9211
	13. Type of Report and Period Covered
12. Sponsoring Agency Name and Address National Aeronautics and Space Administration Ames Research Center Moffett Field, CA 94035	Contractor Report
	14. Sponsoring Agency Code

15. Supplementary Notes

16. Abstract

Four blunted ogive-cylinder missile models with a length-to-diameter ratio of 10.4 have been tested at transonic speeds and large angles of attack in the NASA/Ames Research Center Unitary Plan 11-Foot Transonic Wind Tunnel. The configurations are: body, body with tail panels, body with canards, and body with canards and tails. Forces and moments from the entire model and each of the eight fins were measured over the pitch range of 20° to 50° and 0° to 45° roll. Canard deflection angles between 0° and 15° were tested. Exploratory vapor screen flow visualization testing was also performed. Sample force and moment data are reported along with observations from the vapor screen tests. Comparisons made of body and panel loads for the same models tested previously in the Ames 6- by 6-Foot Wind Tunnel showed good agreement in a small overlapping range of pitch angles.

17. Key Words (Suggested by Author(s))	18. Distribution Statement
high angle-of-attack aerodynamics aerodynamic loads canard configurations missile flight characteristics wind-tunnel test	unlimited Star Category - 02

19. Security Classif. (of this report)	20. Security Classif. (of this page)	21. No. of Pages	22. Price*
UNCLASSIFIED	UNCLASSIFIED	79	$4.00

*For sale by the National Technical Information Service, Springfield, Virginia 22161

NASA-Langley, 1978